INVESTIGATION OF A VENTURI AS A PUMP

APPLICATION TO AN ANTARCTIC SUBLIMATION SYSTEM

BY
MERETTA BOYER
CM 96/13

A THESIS SUBMITTED IN PARTIAL FULFILMENT OF THE REQUIREMENTS FOR THE DEGREE OF

BACHELOR OF ENGINEERING WITH HONOURS

DEPARTMENT OF CIVIL AND MECHANICAL ENGINEERING

UNIVERSITY OF TASMANIA

1996

ABSTRACT

The aim of this thesis was to investigate the operation of a venturi as a pump and to extend the work of a previous study. The study was applied to a sublimation chamber built as a trial at Davis station in the Antarctic which used a venturi style pump to circulate air through the chamber. The investigation consisted of testing the effect of different venturi geometries using a model built previously in the wind tunnel. An attempt was made to verify these results using a finite element analysis program.

Testing of four different diffuser sections showed that 7° was the ideal diffuser angle for a venturi used for this purpose. Investigation showed that the power obtained from the venturi was significantly lower than that obtained from similar sized wind turbines. It was however recognised that the venturi was more suited to this type of application due to it having no moving parts and therefore being more robust than similar sized wind turbines.

The main suggestion arising from this report was that should further improvement be necessary in the chamber design, the incorporation of a wind turbine into the design should be investigated.

ACKNOWLEDGMENTS

I would like to thank my supervisor, Dr A.C. Pittas, for his help and advice over the year and for his input into the project.

Thankyou also to Mr. Jason Roberts for his help during both the wind tunnel testing and computer analysis stages.

I also thank Mr B. Stribec and the other workshop staff for their assistance.

Finally I would like to thank my friends and family for supporting me through some very busy times.

1. CONTENTS

2. INTRODUCTION

The focus of this thesis was to investigate the use of a venturi as a pump, for the particular application in a sublimation drying system in an Antarctic environment. This project contributes to the research conducted previously at ANU and extends the work of a former student of this department, Vanessa Pendelbury.

The aim of the original research conducted at the ANU was to investigate the feasibility of building a facility in Antarctica which was capable of de-hydrating waterlogged timbers. This was conducted after a report by W.R. Ambrose[2] suggested that the Antarctic environment was one of the few suitable environments for the atmospheric freeze-drying to occur naturally.

Freeze drying, also known as sublimation drying, has been identified as the ideal method of drying archaeological waterlogged timber remains such as those recovered from ship-wrecks. This is due to the nature of freeze-drying which is a process whereby the ice in a substance vaporises and passes out of the material without passing through the liquid phase. As a result the warping and cracking which occur when a timber becomes moist is avoided.

Unlike conventional freeze-drying which occurs in a vacuum and is driven by a high pressure differential, this facility was to operate at atmospheric pressure and use the naturally low temperature of the surrounding environment to drive the process. The low relative humidity of the Antarctic environment was also required in order for the sublimation process to be effective. The conditions required for sublimation to occur were that a sufficient quantity of dry air was passed over the surface at a relatively steady rate to enable the diffusion of the water vapour.

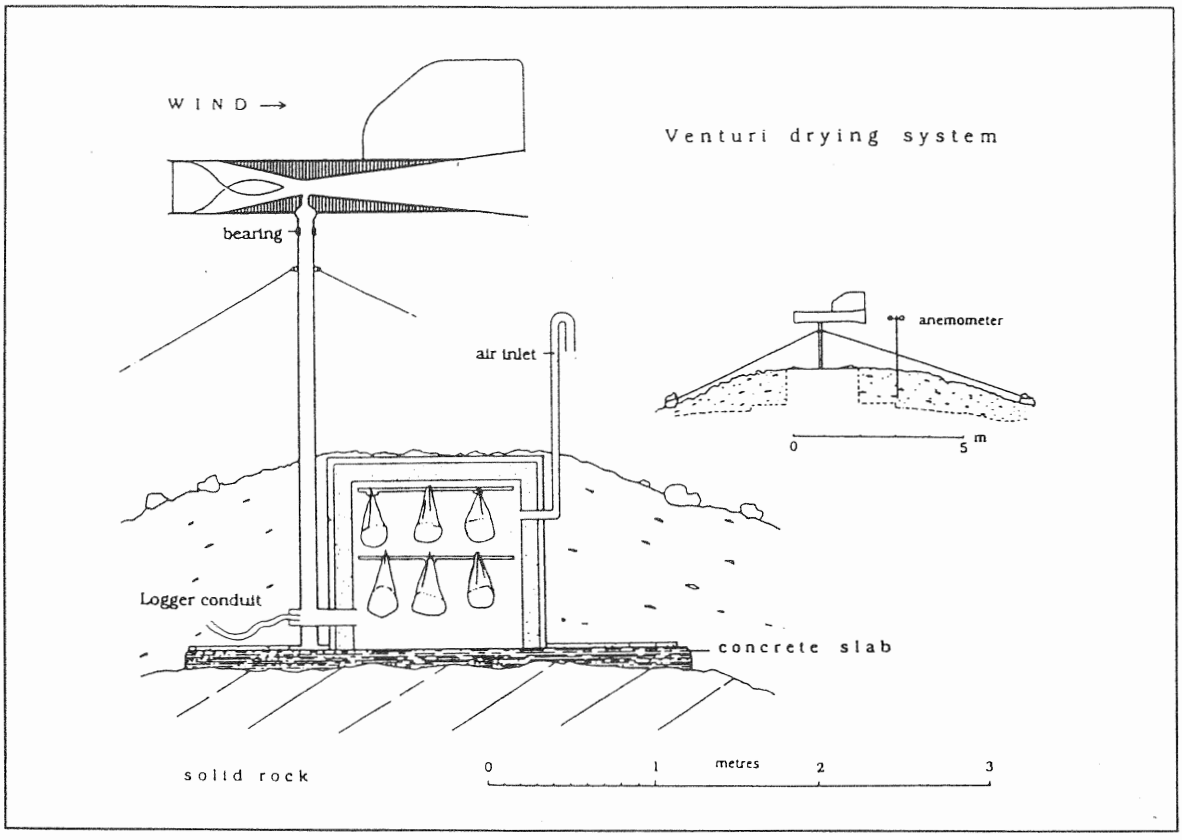

Figure 2.1 - Schematic diagram of venturi drying system

The design of the sublimation facility was subject to a number of criteria. Firstly, due to the remote location of the facility, it was to require low maintenance and be robust in extremes of weather. Past projects located in similar environments had shown that due to the harsh weather conditions, only the most sturdy pieces of equipment had been able to function to their full capacity. It was also necessary that the timber to be dried was protected from wind-borne ice and extremes of temperature. Due to the above zero temperatures occurring in the summer months it was necessary to house the samples below ground in order to dampen the effect of these seasonal temperature changes. The air circulation through the system was generated by a wind tracking venturi pump as shown in figure 2.1. The principle of operation of this pump was that a low pressure region occurred in the throat section of the venturi and that by passing a pipe between a point at atmospheric pressure and this region a suction effect would be generated.

The findings of the study at Davis Station were that the apparatus was satisfactory for its intended purpose, that being dehydrating frozen timber, however it was suggested that the system drew insufficient air through the system to drive the drying process for a reasonable fraction of the year. This implied that with design improvements to the system the efficiency could be improved. The aim of the initial study into this system was to recommend and investigate improvements to the system.

The main aim of this project was to investigate design improvements suggested in the previous study and thus to arrive at an optimum design of a venturi based air pump. These investigations were conducted using a scale model in the wind tunnel and it was attempted to reproduce and analyse these results using the finite element analysis program, FIDAP.

Using the results obtained in the wind tunnel testing, the performance of the venturi was then compared to that of other wind generated turbines.

Figure 2.2 - Sublimation Chamber before and after Installation at Davis Station

3. SUBLIMATION PROCESS

Freeze-drying is possible because under the right conditions, a solid material such as ice can change directly into a gas without first passing through a liquid phase. This process, called sublimation, can be used to gradually remove all ice from food and other biological matter. The theory of freeze-drying is well understood, it is a matter of transport of heat and vapour through a porous solid and there has been much study both theoretically and experimentally, however the transport of both heat and mass depends on pressure in a complex way making theory much more complicated. For sublimation to occur there must be a pressure drop between the vapour pressure of ice in the object and the water vapour pressure in the surrounding air.

The sublimation process was chosen as the ideal method of drying the timber in this situation, the reason for this being that it avoids the cracking and warping which occurs in the timber when it becomes moist.

3.1 Atmospheric freeze drying:

The atmospheric sublimation process can be analysed using the one dimensional model shown in figure 3.1.1 below (from Mellor[5] , pp.69). The sublimation of ice into water vapour requires an increase in internal energy of the molecules, since the temperature of the interior stays relatively constant it is known that there must be a flow of energy from the outside air stream to the sublimating ice surface, this flow is known as the heat of sublimation.

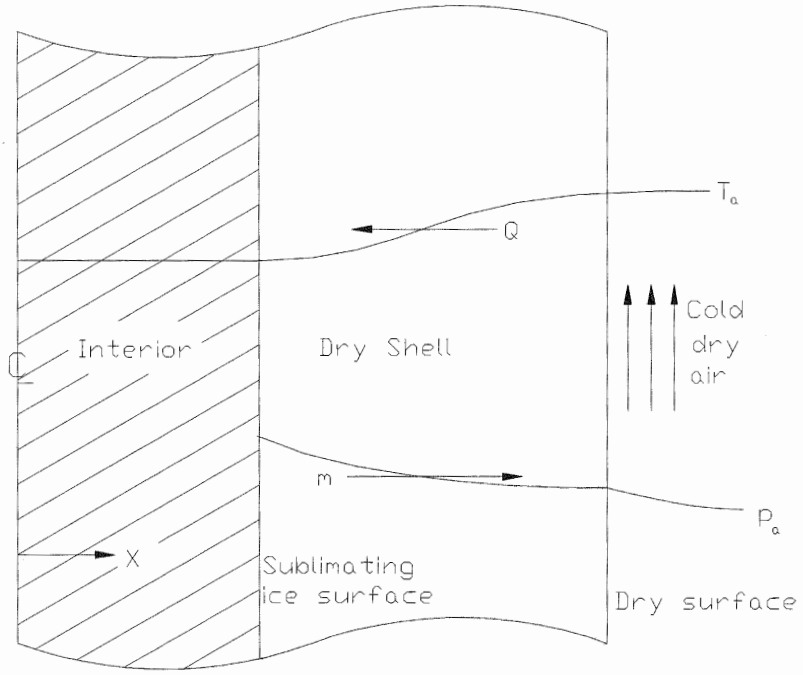

Figure 3.1.1 - One dimensional model of atmospheric freeze-drying

The porous dry shell acts as a thermal insulator which becomes the limiting factor of the process for low pressure freeze-drying methods. In atmospheric freeze-drying processes however, the temperature difference which is the driving potential is significantly larger and therefore reduces the effective resistance of the shell. The major limitation then becomes the maximum rate of water vapour transfer through the dry shell (Ambrose[2] , pp. 249). In both systems the rate of sublimation is also

effected by the permeability and heat conducting properties of the wood. The thickness of the shell increases as drying proceeds, and the heat flow rate decreases proportionately.

The actual rate of mass transfer from the material will be controlled by the heat and mass transfer factors, as shown in the table 3.1.1 following:

Atmosphere	Boundary Layer	Dry Shell	Evaporation Zone	Interior
Mass Transfer	Vapour diffusion $\dot{m}_1$	Flow of vapour $\dot{m}_1$	Vapour diffusion, surface diffusion, $\dot{m}_1 = \dot{m}_0 + \dot{m}_{01}$	
Heat Transfer	Conduction Convection $\dot{q}_1$	Conduction possible, Flow of vapour $\dot{q}_1$	Conduction possible, Flow of vapour $\dot{q}_1 = \dot{q}_{01} + \dot{q}_e$	Conduction $\dot{q}_{01}$

Table 3.1.1 - Modes of energy transfer in the sublimation process

If the external conditions of chamber pressure and temperature of the outer surface are relatively constant, then the ice will assume a temperature that is dependent on the ratio of heat and mass transfer resistances. Although these resistances increase as the thickness of the shell increases, they are both proportional to the thickness, and so the ratio does not change.

Heldman and Hohner (1972), developed a mathematical model which they later verified experimentally (Mellor[5] , pp. 68). From the conservation of energy in a volume dV of the layer they investigated the heat-transfer in a material and suggested

that:

Internal Energy	=	Heat Conduction	+	Energy Input (vapour)	+	Sublimation Heat

giving the equation:

$$\bar{\rho}_d\left(c_d + c_w\right)\frac{\partial T}{\partial t} = \lambda_d \frac{\partial^2 T}{\partial x^2} + K_e \frac{\partial p}{\partial x}\left(c_w \frac{\partial T}{\partial x}\right) + p_i \Delta H \frac{\partial m}{\partial t} \qquad \ldots\ldots(3.1)$$

where:

c_d = specific heat of dry product,

c_w = specific heat of water,

K_e = effective water vapour permeability,

m = moisture content, dry basis,

$\bar{\rho}_d$ = mean density of dry product,

p = vapour pressure,

λ_d = thermal conductivity of dry product,

ρ_d = density of ice,

ΔH = latent heat of sublimation of ice,

T = temperature in the dry layer,

x = distance,

t = time,

One method of solving this equation is to use appropriate boundary transfer conditions at the surface and the interface and thus to find which of these has the higher resistance to the heat transfer. At the evaporation interface we get:

$$\rho_i \Delta H\left(m_0 - m_f\right)\frac{dX}{dt} = -\lambda_d\left(\frac{\partial T}{\partial x}\right)_{x=X} + \rho_i X c_i\left(1 + m_0\right)\frac{\partial T_i}{\partial t} \qquad \ldots\ldots(3.2)$$

Where

m_0 = initial moisture content of dry basis

m_f = final moisture content of dry basis

λ_i = thermal conductivity of ice

T_i = ice temperature

X subscript $\Rightarrow$ interface

(see Appendix C)

and at the dry surface we obtain the boundary condition:

$$-\lambda_d\left(\frac{\partial T}{\partial t}\right)_{x=s} = h\left(T - T_a\right) \qquad \ldots\ldots(3.3)$$

where

m_0 = initial moisture content of dry basis

m_f = final moisture content of dry basis

λ_i = thermal conductivity of ice

c_i = specific heat of ice

T_i = ice temperature

T_a = external temperature

h = surface heat transfer coefficient

X subscript $\Rightarrow$ interface

s subscript $\Rightarrow$ surface

There has been extensive investigation into atmospheric freeze-drying for use in the food industry but it has been found impractical for this purpose due to the slow rate of drying obtained. This is mainly due to the resistance to heat transfer into the material and the low driving force (in conventional freeze-drying the driving force is the pressure differential due to partially evacuated surroundings which overcomes the resistance more effectively). Studies have shown however that the drying rate for atmospheric freeze drying of foodstuffs is independent of the velocity of air flow over the surface for air velocity greater than 0.5 ms^{-1}. It is assumed here that this

principle can also be applied to timber products due to their similar fibrous nature.

It must be considered that the drying speed of the timber will be somewhat effected by its longitudinal grain making results difficult to predict. The long cells are designed to carry fluids in the longitudinal direction, therefore the resistance to the flow of both heat and vapour are less along the grain than across the grain. Since the timbers are generally cut along the grain this timber will probably have a much higher resistance than less fibrous matter.

4. DESIGN OF THE VENTURI MODEL

The scale model of the venturi pump was built during the previous study and satisfied geometric similarity. For a wind tunnel testing speed of approx 20 ms^{-1} kinematic and dynamic similarity was to be achieved. A comparison was made between this design and recommendations made in BS 1042, however it was noted that as the design of the venturi was intended as a pump rather than as a flow measurement device as in BS 1042, the deviations from the code described may not have been important. The dimensions and notation used in the code are shown in figure 4.1.

Some deviations noted were the angle of convergence which was 30° rather than the recommended 21 ±1° and the length of the convergent section of 2.0(D-d) rather than 2.7(D-d). The code also recommended the length of the venturi throat to be equal its diameter while in the prototype the length of the throat was 100 mm while the diameter was 90 mm. The final deviation noted and the one considered the most critical was the angle of the diffuser. This was 15° in the original prototype while the British standards recommended an angle of 7°.

4.1 Testing of Various Venturi Models:

The effects of the above deviation were experimentally investigated by building a model allowing various diffuser angles to be tested in the wind tunnel in order to compare results. The model was built as a scale replica of the original design for the sublimation chamber. The original prototype however was altered to include an inlet cylinder and a pre-rotation vane at the inlet. The characteristics of the venturi model have been outlined in diagram 4.1.1.

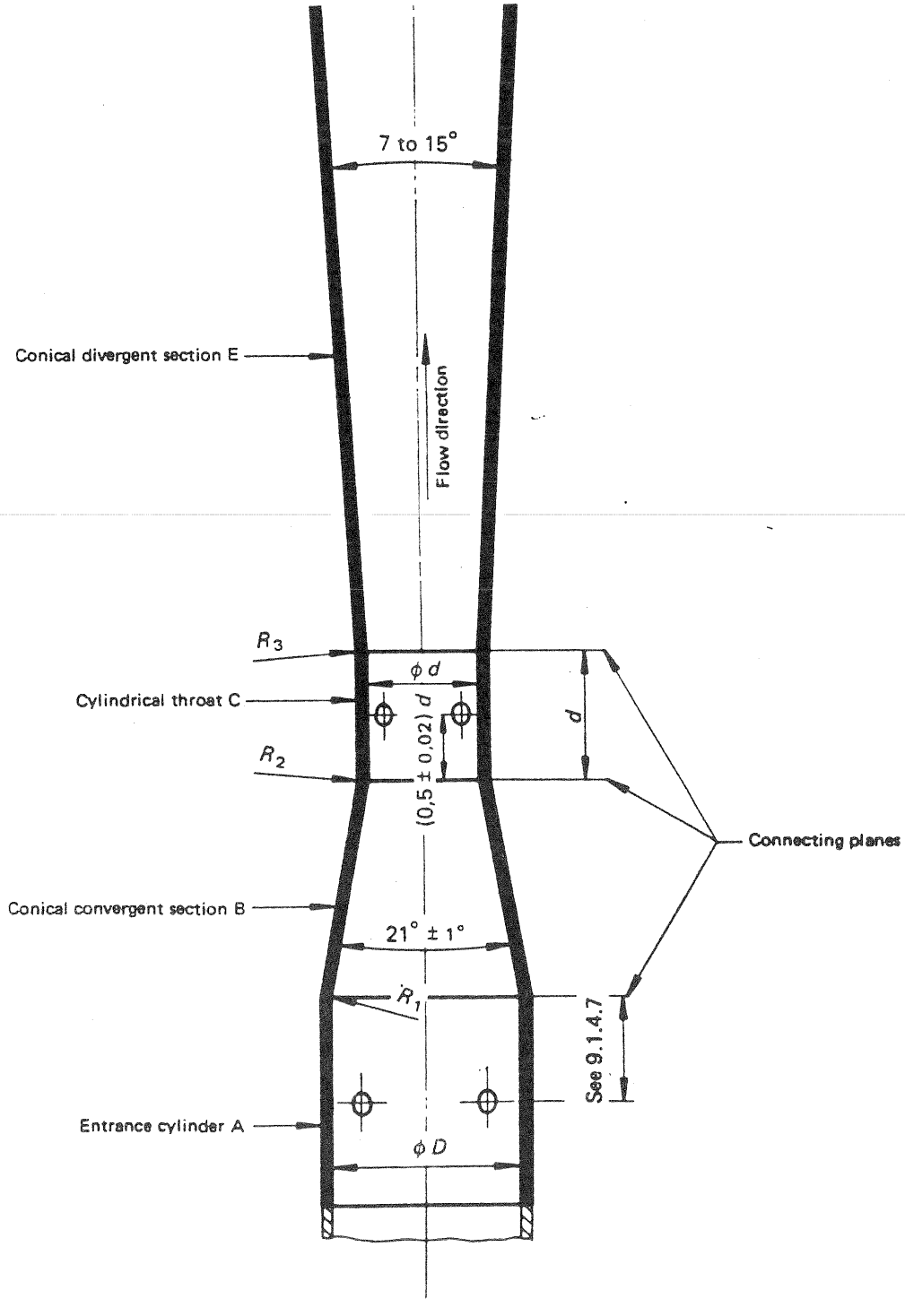

FIGURE 7 — Geometric profile of the classical venturi tube

BS 1042

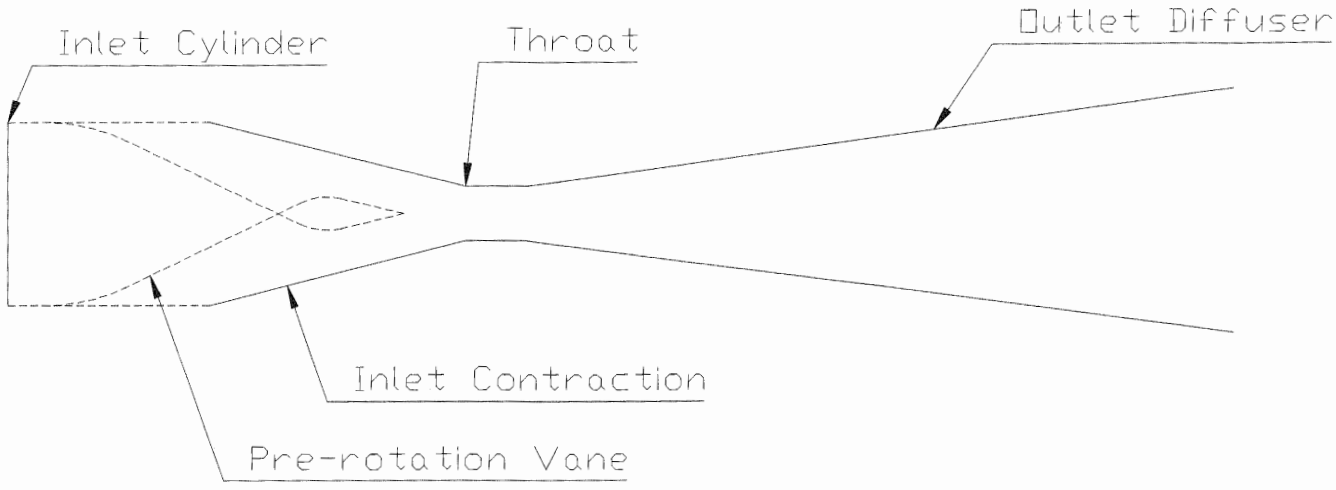

Figure 4.1.1 - Characteristics of the venturi model - later additions have been added in dotted lines.

It was predicted and shown in former testing that the venturi diffuser angle of 15° used in the original design was too large and that better results were obtained using an angle of 7°. After verification of these results, further investigation was conducted into the optimum venturi angle by testing diffuser angles of 10° and 5 °.

An inlet cylinder was attached to the model and the tests were repeated for the 15° and 7° diffusers. Finally the flow direction around the venturi inlet and exit was investigated using a tuff.

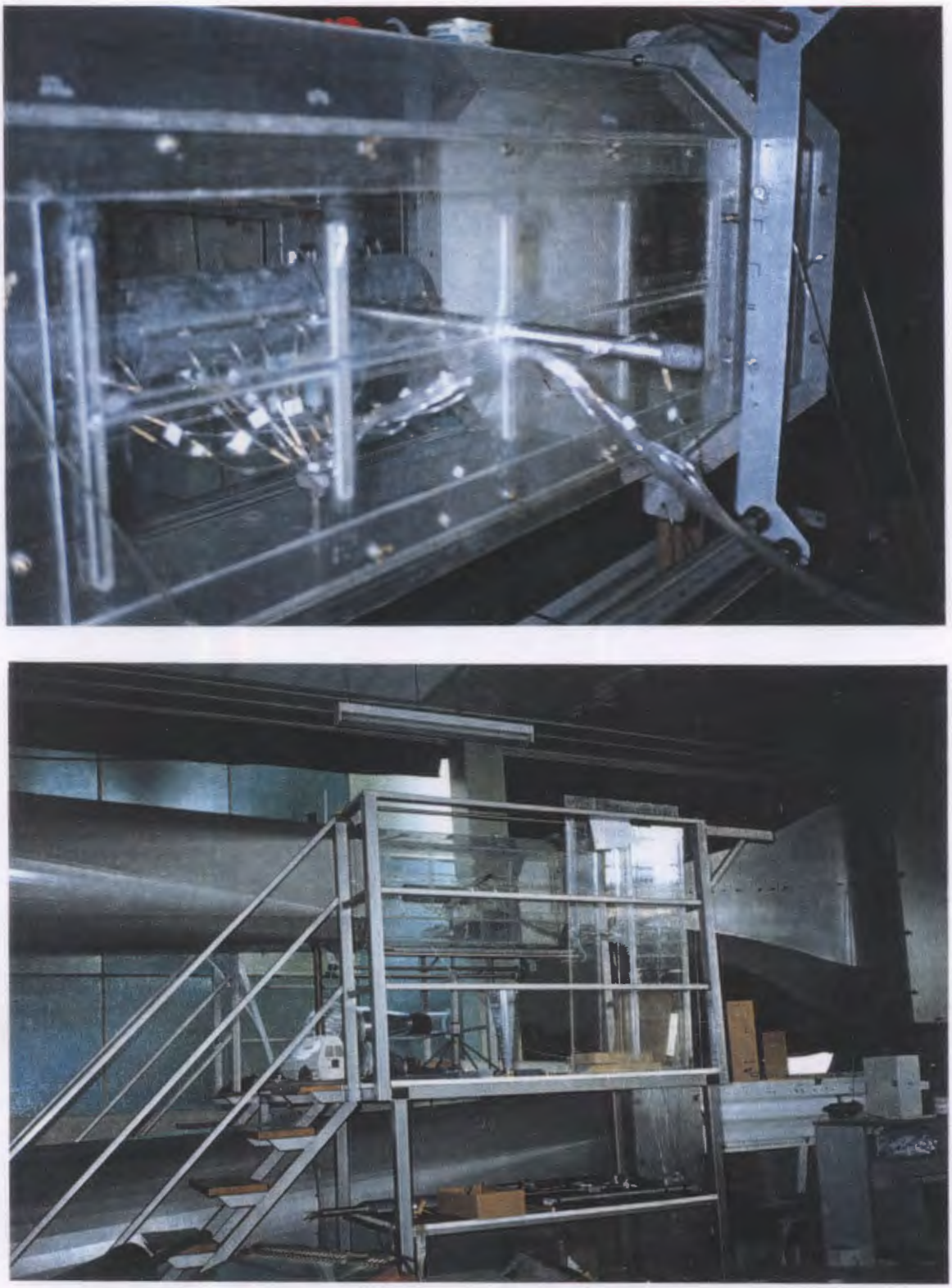

Figure 4.2.1 - Photos of model set up in wind tunnel

4.2 Performance of Venturi Model

From the initial tests for the 15° and the 7° diffuser it was established that the pressure distribution was radially symmetric for both sections. This was true with no off-take flow and with full flow. The radial distribution of pressure for the 15° diffuser with full off-take flow is shown in figure 4.2.1. As a result of these tests the pressures along the venturi could be taken as an average of those measured around the model.

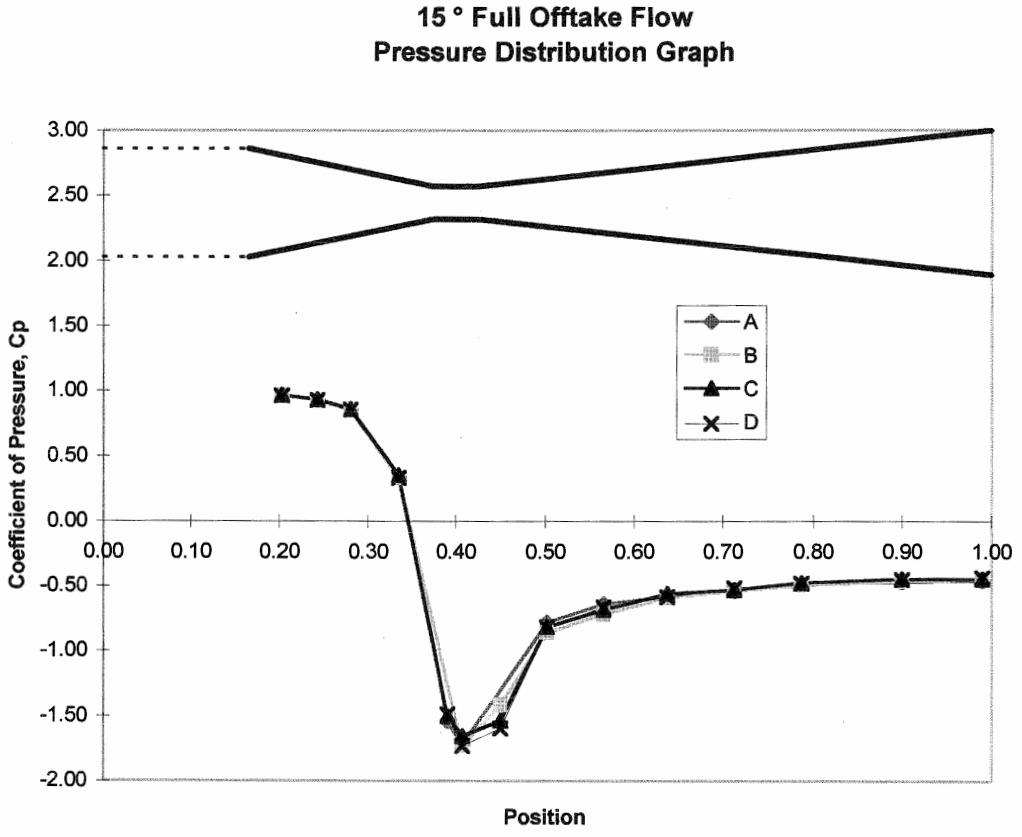

Figure 4.2.1 Axial distribution of pressure around model

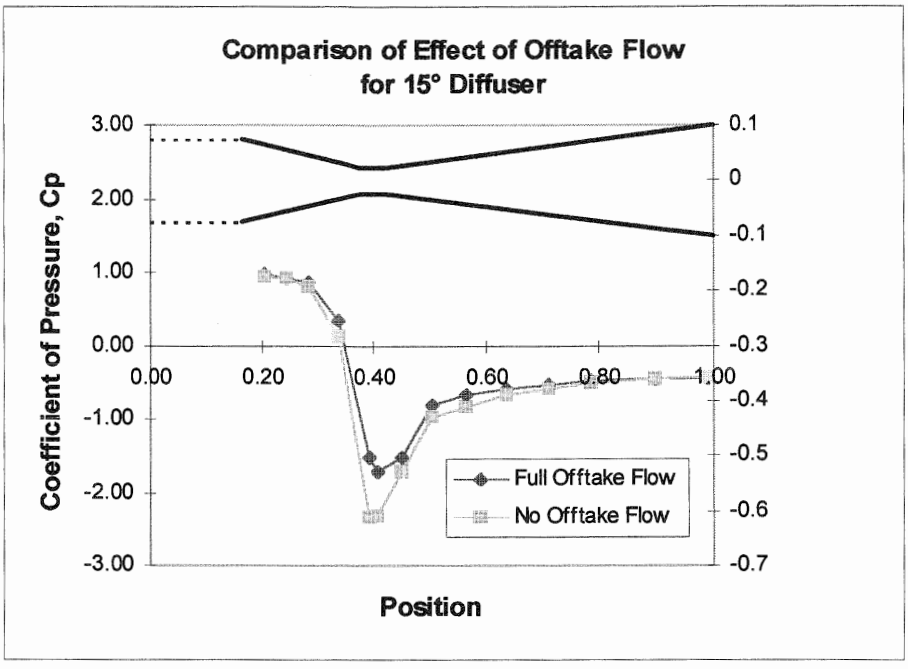

Figure 4.2.2 - Comparison of off-take flow for 15° diffuser

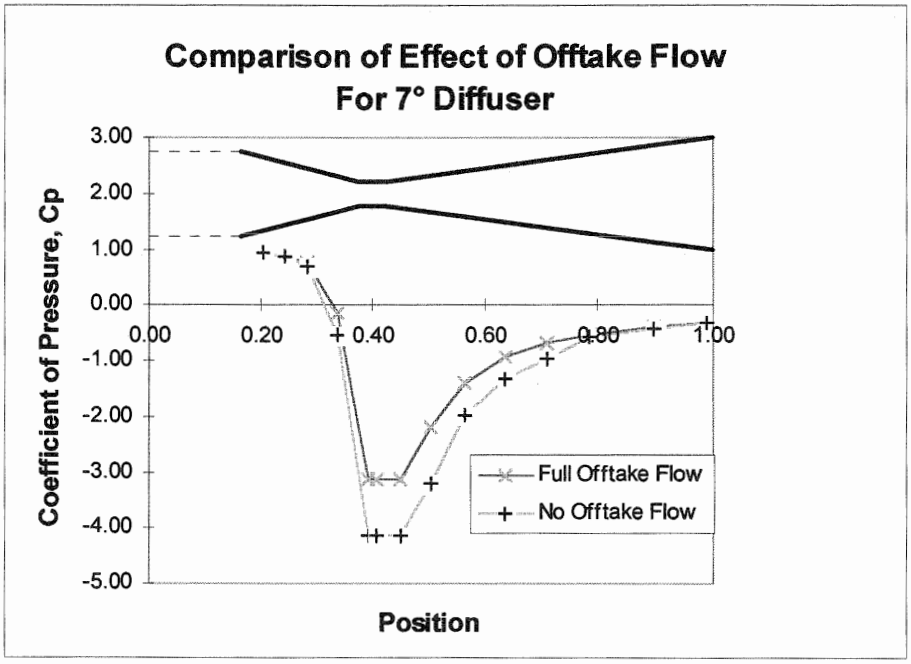

Figure 4.2.3 - Comparison of off-take flow for 7° diffuser

The results have been non-dimensionalised in order to allow comparison between different tests to be independent of tunnel wind speed and atmospheric conditions. This was done by dividing by the static tunnel tapping. The effects due to the testing being conducted in a wind tunnel were also removed by accounting for solid and wake blockage as described in Appendix D.

The effects of off-take flow on pressure coefficient were compared for each diffuser angle tested. It was found that the 7° diffuser produced the lowest pressure both with and without off-take flow with -4.15 times the static pressure tapping for no off-take flow and a coefficient of -3.11 with off-take flow. This shows as expected that an angle of 7° is a great deal more efficient than the initial prototype angle of 15°. For all angles the minimum pressure coefficient was recorded with no off-take flow. This was as expected with an increase in pressure of about 20 % for full off-take flow. This effect was apparent as soon as any off-take flow was introduced and would most likely be due to boundary layer thickening in the throat. The effect of off-take flow for the 15° and 7° diffusers are shown in figures 4.2.2 and 4.2.3 respectively.

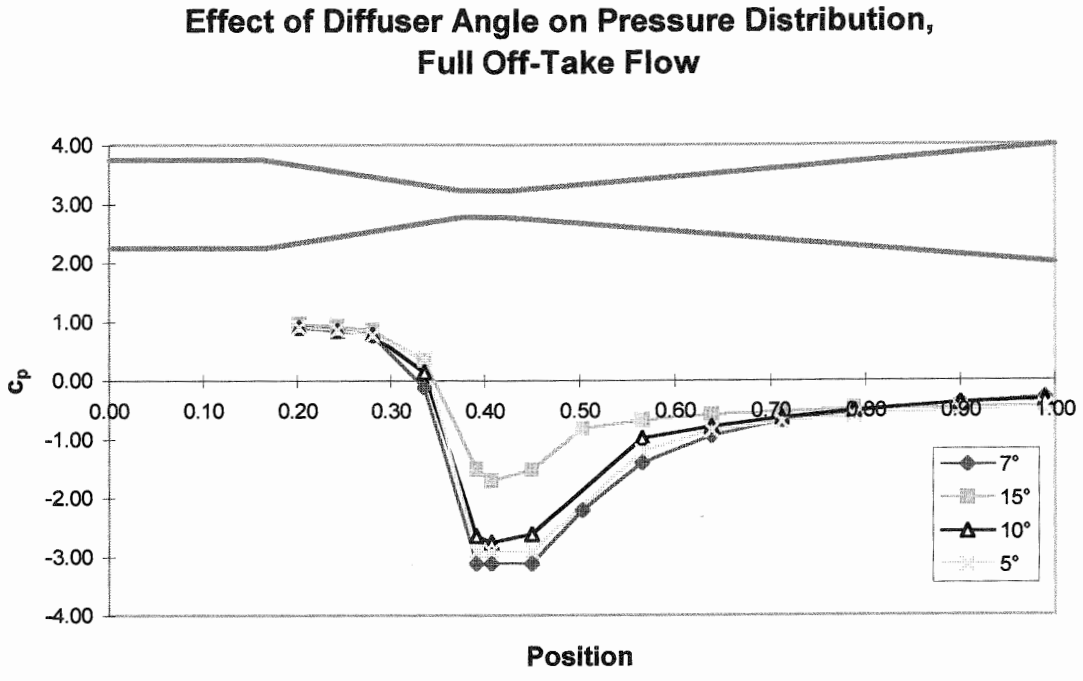

Figure 4.2.4 - Effect of angle on pressure along venturi for full off-take flow

Figure 4.2.4 illustrates the difference in pressure distribution for varying diffuser angles. It is interesting to note that the minimum pressures developed in the 5° and 10° degree diffusers are close to those developed in the 7° diffuser with the minimum in the 15° diffuser some 45% smaller. This will imply that any diffuser angle in the region of 5° to 10° will give significantly improved results to those using the original scaled prototype.

The off-take flow was measured using a bellmouth nozzle (as shown in appendix C) however it must be noted that the flow measured can be used as a guide only due to the roughness of the measurements. The main reasons for the inaccuracies can be seen by comparison with BS 1042 for nozzle design for the purpose of flow measurement. The main discrepancies from this code are the distance from the nozzle of the first pressure tapping, the shape of the nozzle and the diameter of the downstream pipe. BS 1042 recommends a minimum pipe diameter of 50 mm on the

downstream side of the nozzle whereas the diameter of the off-take pipe was 8 mm. The standards do not recommend a flow measurement method for a pipe of this diameter. Due to the fact that the flow rates were required for a guide only it was decided that the bellmouth nozzle was sufficient.

The flow rates measured using this technique are shown in table 4.2.1 below:

Diffuser Angle	15°	7°	10°	5°
Measured Flow	0.64 l/s	1.12 l/s	0.94 l/s	0.86 l/s

Table 4.2.1 - Off-take flow rate measured with varying diffuser angles

It can thus be seen that although the pressure at the throat was not significantly different for the 7° diffuser to that of the 5° and 10° diffusers, the flow rate is significantly higher. This implies that the flow rate through the system is highly dependent on the pressure at the venturi throat.

For the second part of the testing, a cylinder was placed at the inlet of the venturi, due to the specifications placed on the inlet cylinder by BS 1042 it was expected that this cylinder would have a large effect on the performance of the venturi as a pump. The results did not show a significant lowering of throat pressure as expected but instead showed a faster recovery to the atmospheric pressure. The fast recovery to pipe pressure is important for a venturi which is used for measuring flow-rates, however, in this particular application it would not be expected to effect the measured off-take flow. The minimum cylinder length suggested in BS 1042 is therefore likely not to effect results for the venturi being used as a pump.

It was found that although less suction at the venturi throat should imply a less efficient system, the flow rate measured was in fact higher than that measured without the cylinder for both the 15° and 7° diffusers. This could show that the off-take flow rate is not solely dependent on the pressure at the off-take point, but is partly dependent on the flow pattern inside the throat of the venturi meter. This could also be caused by changes in other variables since the flow rate was not calculated as a non-dimensional variable.

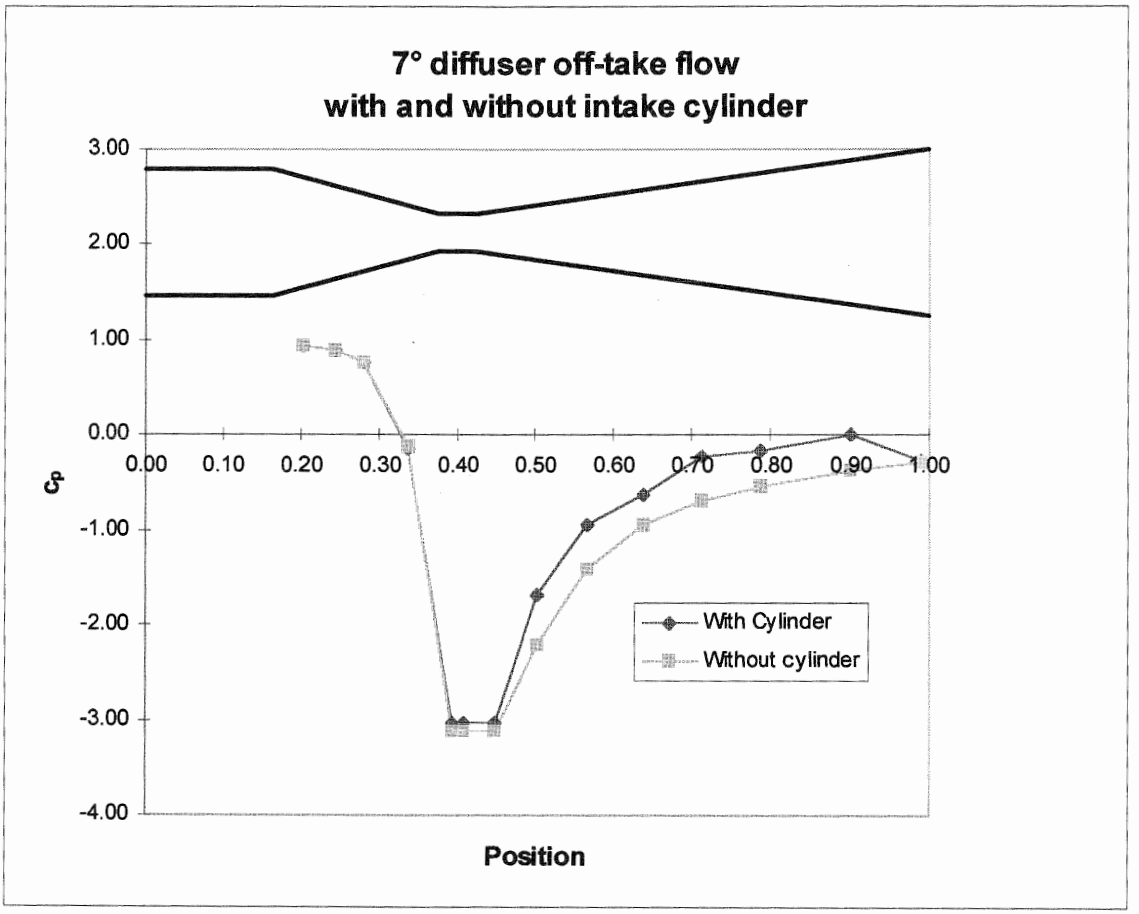

Figure 4.2.5 - Effect of inlet cylinder on pressure distribution

The final part of the testing in the wind tunnel involved investigating the direction of the flow around the venturi using tufts. This experiment was conducted on the 15° diffuser only. The flow at the outlet of the venturi was turbulent, this implies that the flow through the venturi may not have been as predictable as expected. The results obtained agreed with those obtained using computer analysis and discussed in section 5.2. The results from the FIDAP analysis for the 15° diffuser without an inlet cylinder are shown in figure 4.2.6. It can be seen in figure 4.2.6 that the majority of the flow actually flows around the venturi rather than through it, this is a factor which must be considered in the use of a venturi as a pump and in consideration of whether the pump is getting the maximum energy possible from the flow under the conditions.

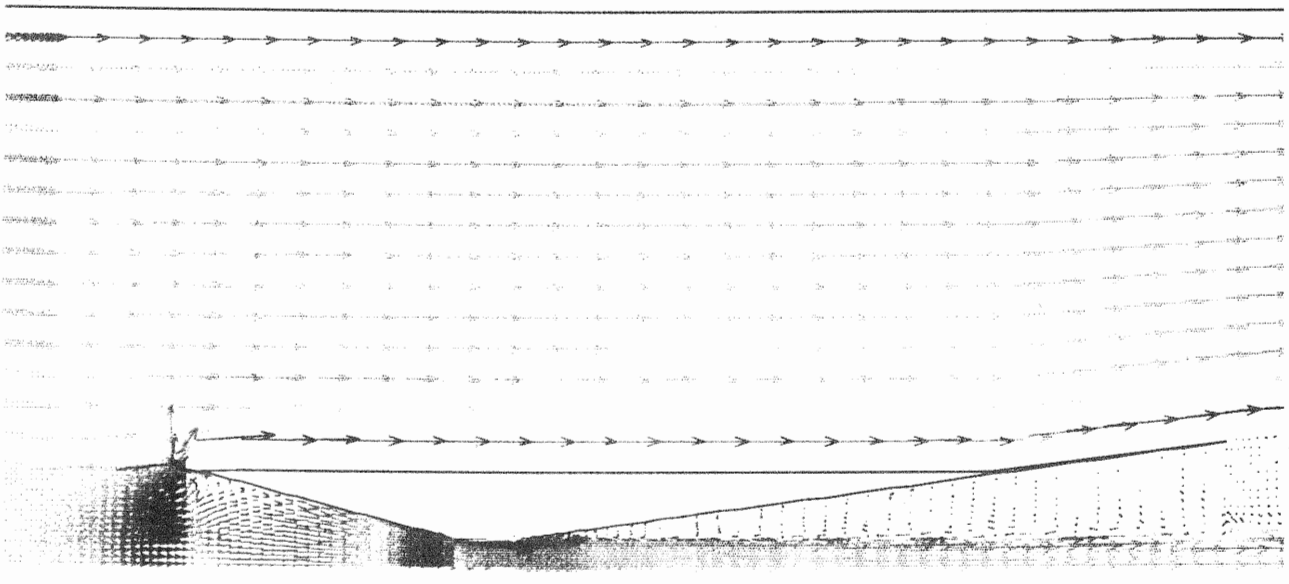

Figure 4.2.6 - Flow pattern expected around 15° diffuser with no inlet cylinder

It should be noted that the testing in the wind tunnel was not performed under ideal situations, the main factor which could contribute to inaccuracies in the results was the suction of air from outside the wind tunnel into the wind tunnel through the off-take pipe. While this was not large enough to have greatly effect results, it may have affected the blockage corrected factors since these were derived using the principles of continuity.

4.3 COMPARISON TO PUMPS AND FANS

Due to the fact that the pump runs using wind energy and that this energy has a very low grade it is not feasible to compare the efficiency of this pump with other pumps and fans using electrical energy. However a comparison can be made between this pump to other turbines in similar situations, the most obvious of these being windmills. The performance of the venturi pump could be expected to be significantly higher than that of the windmill due to the nature of the energy produced and the losses involved. While a wind generator tends to convert wind energy to electrical or mechanical energy involving transmission and losses the venturi pump is simply using the flow of a substance to generate another flow, the only losses are through wall friction and turbulence losses.

The power in the wind is contained in the form of kinetic energy. This energy is of a low grade and therefore difficult to convert to a useable form with high efficiency. The rate of energy passing through a cross-sectional area, A, can be written as:

$$P = \tfrac{1}{2}U^2 . AU\rho = \tfrac{1}{2}\rho AU^3 \qquad \text{.....(4.3.1)}$$

Since the mass flow rate of air through the area = $AU\rho$ and the kinetic energy of a unit mass having velocity $U = \tfrac{1}{2}U^2$. From equation (4.3.1) it can be seen that the wind power is highly dependent on the wind speed.

If all the energy could be extracted from the wind then the air particles would have no velocity after the collector device. Thus it is not possible to harness all energy from the wind. It has been shown that the maximum possible proportion of power which can be utilised and converted to other forms of energy from the wind is 16/27 of the available wind energy. This factor is called the Betz coefficient.

The power coefficient, C_P, of an aerogenerator is defined as the ratio of wind power available to that generated, this is generally written as:

$$C_P = \frac{P}{\frac{1}{2}\rho A U^3} \qquad .....(4.3.2)$$

where P is the power generated by an aerogenerator and can be written as $P = \Delta p_b Q$ if Δp_b is the pressure differential across the bellmouth nozzle.

The velocity of the flow in the wind tunnel can be found as $p_1 - p_2 = \frac{1}{2}\rho U^2$ and the flow-rate can be found using the equation: $Q = C_{DN} A_o \sqrt{\frac{2\Delta p_b}{\rho}}$, where C_{DN} is the correction factor as given by BS1042 and A_0 is the area of the off-take tube at the pressure tapping.

Thus it can be shown that:

$$C_P = C_{DN} \frac{A_0}{A_i} \Delta c_{pth} \sqrt{\Delta c_{pb}} \qquad .....(4.3.3)$$

where Δc_{pth} is the difference in pressure coefficients between the throat and the atmosphere

Δc_{pb} is the difference in pressure coefficients across the bellmouth nozzle and

A_0/A_i is the ratio of the areas of the off-take tube and the venturi intake section.

Using equation 4.3.3, C_P can be obtained for each test model. The maximum C_P found was 0.031, this occurred with a diffuser angle of 7° as expected. This can be compared to that of other types of wind powered turbines shown in figure 4.3.1. The resulting value of C_P is very small considering the possible losses involved, the most likely explanation for this is that the majority of the wind does not flow into the face

of the venturi but rather around it. Thus it can be seen that the pump is obviously not obtaining full potential from the wind.

This study highlights the main problem with the use of a venturi as a pump. The venturi was never designed as a pump but as a flow measuring device. It was not designed to give a high suction pressure and any introduced flow has a large effect on the driving pressure, as has been shown experimentally. The ideal wind powered pump of this style would be one which was specifically designed to develop a low pressure region and to obtain the most energy from the surrounding wind.

It should however be kept in mind that the venturi operates as a pump with no moving parts. This makes it many times more robust than other pumps and which makes it a suitable design for use in the extreme conditions discussed. Another reason for the choice of a venturi is that it created a suction effect through the system. This was expected to produce a 10% drop in pressure in the chamber to improve the sublimation process however in actual fact the design produced only a 1% drop. This means that the designers would have been better to have designed to system to provide minimum resistance air flow rather than attempting to create a suction in the chamber. It is worth investigating the most robust of turbines and comparing their performance to those of the venturi style pump.

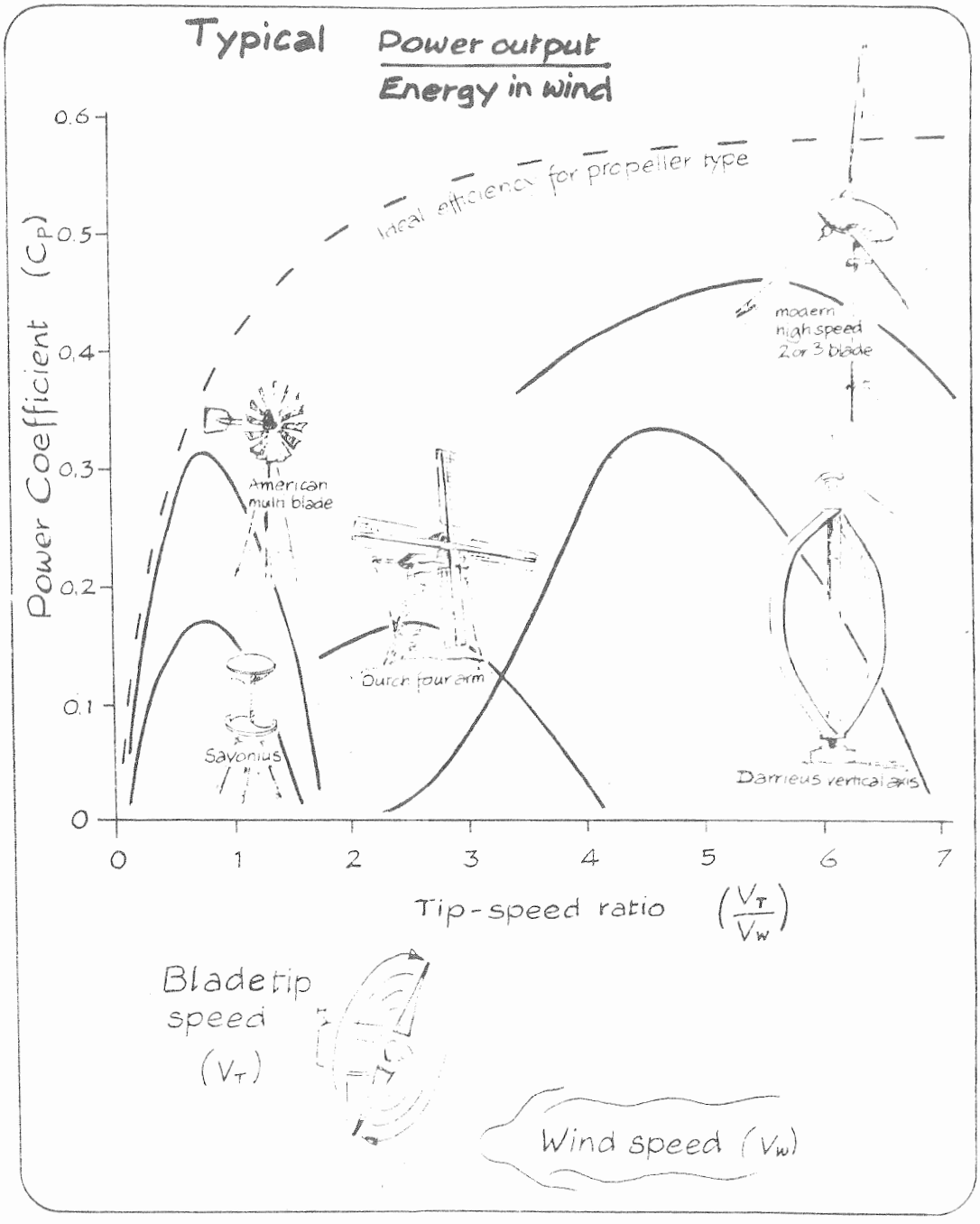

Figure 4.3.1 - Power coefficients for various wind turbines

From Twidell [97]

5. OPTIMUM SOLUTION USING COMPUTER ANALYSIS

FIDAP - Fluid Dynamics Analysis Package

FIDAP is a finite element fluid analysis package, capable of analysing the behaviour of fluids including the effects of heat and mass transfer. FIDAP utilises the fundamental equations of fluid flow, momentum conservation, mass conservation and energy conservation as well as the equation of state to model the behaviour of a fluid. FIDAP can of deal both with compressible and incompressible fluids, turbulence and two phase flow and is capable of using various reference frames.

The aim of this task was to attempt to verify model testing results using FIDAP and in the process to investigate the flow through the model.

The FIDAP problem consisted of computer representation of the scale model set-up in the wind tunnel with similar atmospheric conditions. By defining the problem in this manner the results obtained should agree with those obtained in the wind tunnel tests.

In order to simplify the problem for solution using FIDAP several assumptions were made, these included assuming that the fluid was incompressible and therefore neglecting the effects of buoyancy, it was also assumed that the fluid properties were not temperature or species dependent and that the fluid had constant viscosity. By doing this it was possible to neglect the energy equation, the species equation and the buoyancy term in the momentum equation and thus to use this equation in the Navier-Stokes form. By using the assumption of axial symmetry and assuming laminar flow the solution method was greatly simplified. The initial solution was obtained using Stokes theorem and using an iterative process a final result was obtained. The methods used to obtain these results have been described in appendix G. It is important to realise that the use of a finite element analysis package is generally not

expected to correlate with actual results due to the large number of assumptions and approximations made.

The analysis did not allow for an off-take flow and was run for four different cases:

1. 15° diffuser with no inlet cylinder

2. 7° diffuser with no inlet cylinder

3. 15° diffuser with inlet cylinder

4. 7° diffuser with inlet cylinder

The results obtained have been included in appendix A. The solutions are not reliable as the program only converged to a final solution in one case, that of the 7° diffuser with no inlet cylinder. The other cases however are assumed to be reasonably close to the final solution given that the solutions converged to a very small error (approx 0.0001 of the error from the first iteration).

5.1 Computation of Suction Characteristics

Using the results obtained using the FIDAP package it was possible to plot the change in pressure along the venturi wall. These results did not agree with those obtained in the wind tunnel tests. The result for the convergent solution (7° diffuser with no inlet cylinder) gave a maximum suction coefficient of 1.90 when divided by the pressure at entrance to the venturi. This can be compared to that obtained experimentally of 4.0. The results for other cases gave suction coefficients of 0.2-0.3 which are a great deal less than those measured.

The main explanation for these discrepancies would be that the solution not converging had a significant effect on the values for pressure expected in the system. The variation of results obtained for case 2 could be due to inaccuracies in the assumptions made. These would include the use of a circular wind tunnel instead of a square tunnel and the assumption of laminar flow. The errors due to these assumptions would not be expected to effect results to this extent however the accuracy of the results of a computer analysis program can really only be expected to be used as a guide.

5.2 Computer Investigation of Flow Behaviour

The results from the computer analysis show that the main streamlines of the fluid actually flow around the venturi meter rather than through it. The results for the 15° diffuser without the inlet cylinder are shown in figure 5.2.1. These effects are expected to be more prevalent in the actual system where there are no wall effects to be considered. These flow patterns were investigated in the wind tunnel tests and the results were found to correlate well. The irregular flow observed at the exit from the venturi in the wind tunnel tests were also obtained for all solutions but were least obvious in the convergent solution.

It was noticed that the wake from the object was large. This was not expected to effect the operation of the venturi in the sublimation system but may have effected the results obtained in the wind tunnel.

15° Diffuser Without Inlet Cylinder

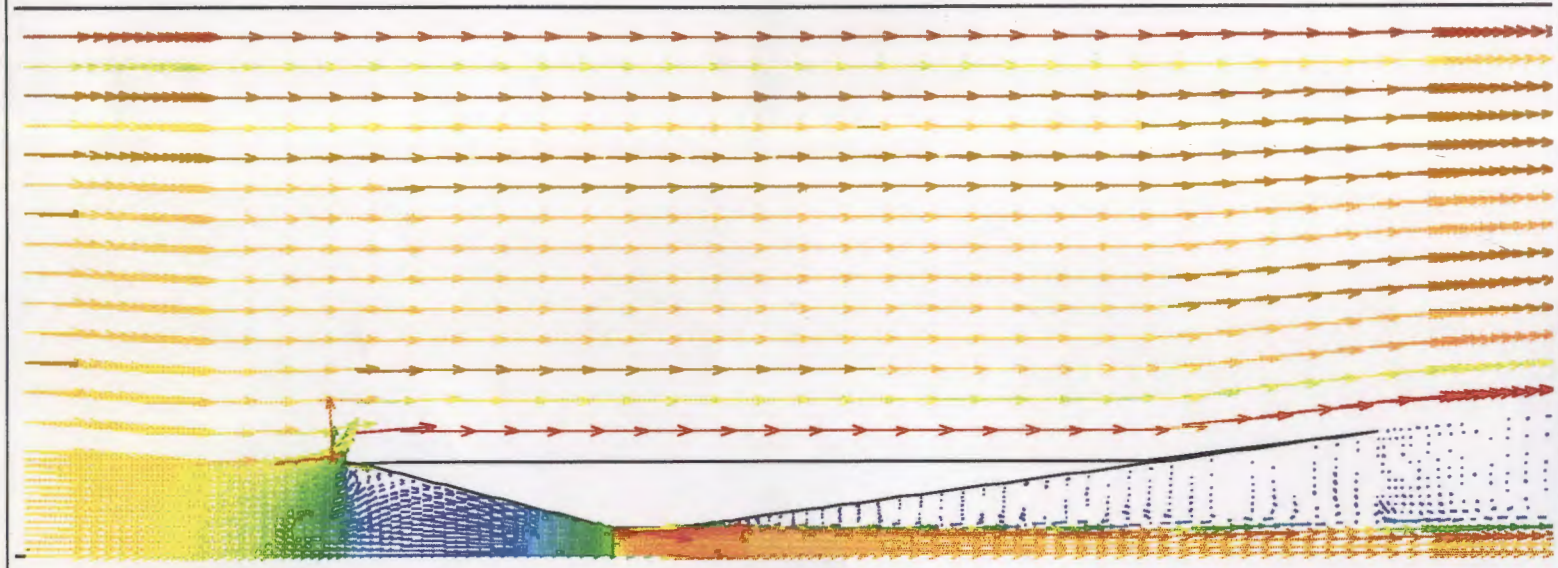

VELOCITY
VECTOR PLOT

SCALE FACTOR
0.5000E+02

REFER. VECTOR
→0.2335E+02

MAX.VEC.PLOT'D
0.2320E+02
AT NODE 5367

COLOR CODE:
VELOCITY

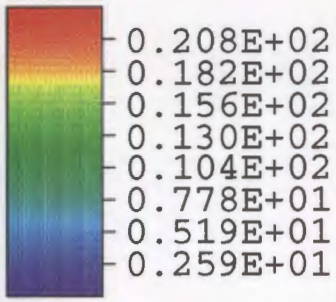

SCREEN LIMITS
ZMIN -.766E-01
ZMAX 0.763E+00
RMIN -.333E+00
RMAX 0.412E+00

FIDAP 7.51
4 Nov 96
10:18:13

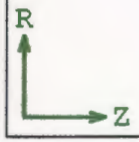

6. DESIGN OF THE INTAKE SECTION

6.1 Expected performance of the system

From the results obtained in section 4.2 we can predict the performance of the system. using the pressure head obtained using the scale model, and assuming the losses obtained in the previous study. The pressure head obtained in the scaled down model was 0.236 m (air), this must then be multiplied by the scaling factor of 3 to obtain the expected head in the full size prototype.

The total of the losses in a system can be written as $\Delta h_{total} = \frac{\sum k_i v_i^2}{2g}$ where k_i is the friction loss and v_i is the velocity of fluid flow through each element of the system. Now since $v = \frac{4Q}{\pi D^2}$ for a cylindrical pipe, as long as the flow through the system is constant, it can be written that:

$$\Delta h_{total} = \frac{8Q^2}{\pi^2 g} \sum \frac{k_i}{D_i^4} \quad \text{.....(6.1.1)}$$

In the original system the flow was divided between two pipes for part of the inlet section. Therefore due to the fact that $\Delta h \propto Q^2$, eq. (6.1.1),we know that the head loss over this section is equal to 1/4 the head loss over the equivalent section with full flow. Since $\Delta h \propto k_i$ we can introduce the equivalent friction loss $k^*_i = \frac{k_i}{4}$ and rearrange eq. (6.1.1) to obtain:

$$Q = \sqrt{\tfrac{1}{8} \Delta h_{total} \pi^2 g \sum \frac{D_i^4}{k^*_i}} \quad \text{.....(6.1.2)}$$

Now from figure 6.1.1 (Pendlebury[6]) and from we can obtain a value for $\sum \frac{D_i^4}{k^*_i}$ through the system. It is necessary to assume a loss through the chamber itself, this is taken to be 20% of the other losses which is a reasonable estimate. From

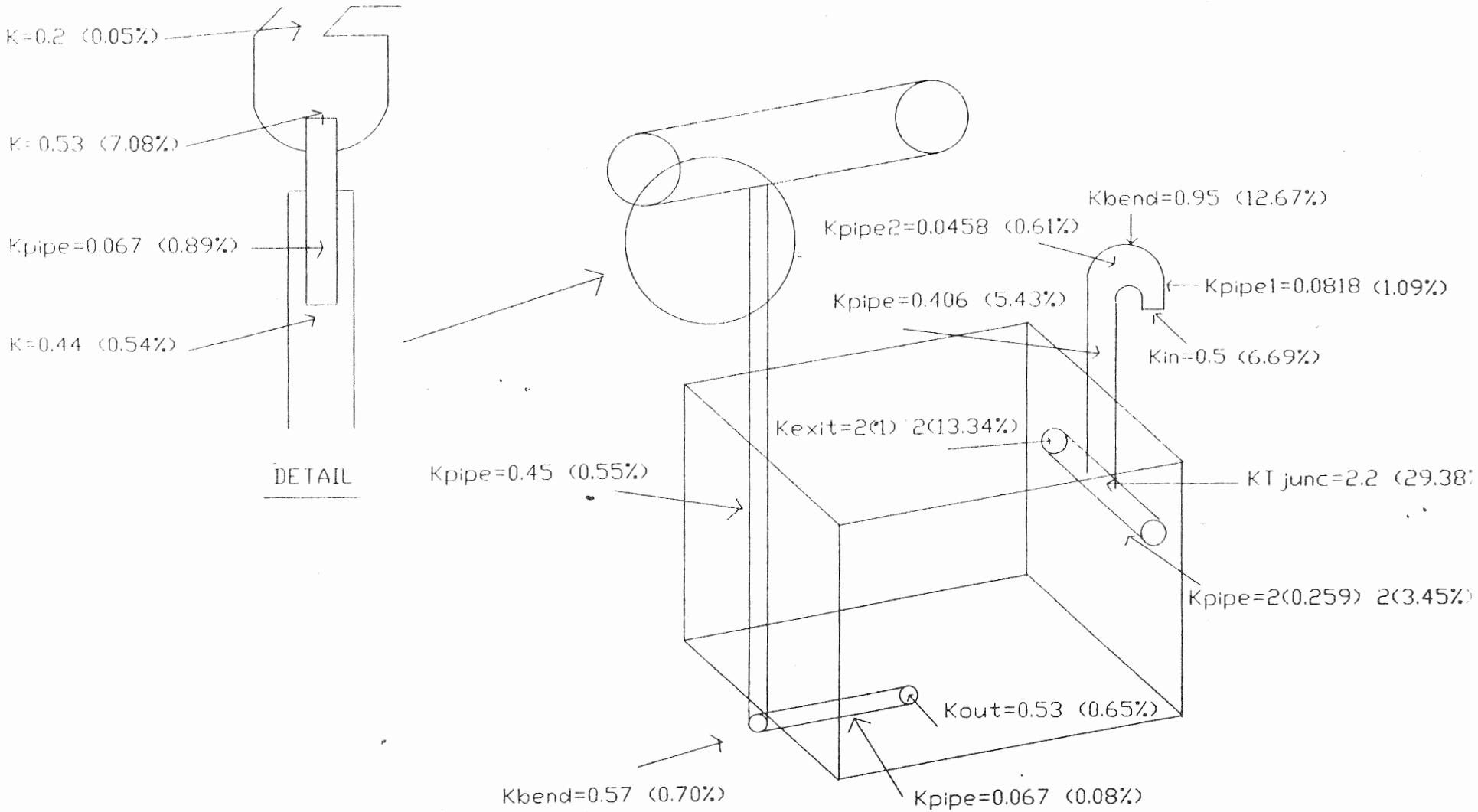

Figure 6.1.1 - Losses Associated with the Drying System

Pendlebury [6]

appendix N we get $\sum \frac{D_i^4}{k^*_i} = 6.59 \times 10^5$, this gives us Q = 5.55 l/s

Since this flow is divided and half is inserted at each end of a chamber of dimensions 1m × 1m × 2m we can assume that we have 0.00278 m^3s^{-1} of flow passing diagonally through a space of 1m × 1m × 1m. It can be seen that this flow will not naturally provide a velocity of 0.5 ms^{-1} over the timber in the chamber. After the chamber was built extra circulation fans were produced however even with these fans the velocity is unlikely to get this high. It can thus be assumed that any improvements in the design of the drying chamber will improve the performance of the system.

One possible area for improvement in the system would be to increase circulation inside the chamber, this would increase the velocity of wind-speed over the samples. However the most obvious place for improvement in the system would be to reduce the resistance to flow of the system therefore allowing more air to pass through the system.

The largest resistances in the system were found to be the gooseneck inlet at the entrance to the system and the T-junction dividing the flow, these will be looked at as the most likely places for general improvements to the system.

6.2 Alternatives to the gooseneck inlet design

The original design prototype consisted of a gooseneck inlet, this was shaped to prevent snow and ice entering the drying chamber. Although assumably successful in this it was identified as contributing to a large proportion of the pressure loss in the system. It was suggested that the design of this section could be improved without changing the important feature of not letting snow and ice into the system.

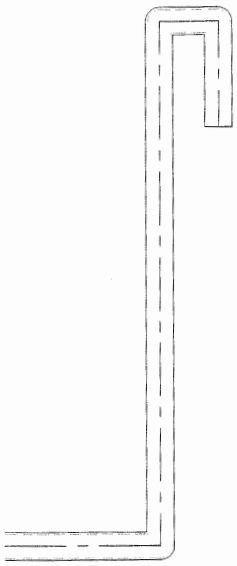

Figure 6.1.1 - original design for inlet

Further investigation was conducted into ideal design of the intake section. Since it was shown that the pressure inside the drying chamber was not significantly below atmospheric pressure to have any noticeable effect on the drying effectiveness. It was decided that there was no reason why the system should not pump air into the chamber at the inlet, thus a model including a fan in the inlet was designed. The main criteria for this design is that the pressure inside the chamber should not high enough to significantly decrease the drying efficiency of the system.

The ideal model would be one in which the gain in head over the inlet pump was equal to the head loss through the inlet part of the system and the pumping head in the outlet side was equal to the head loss through the outlet side of the system. However this is not easy to design for since the head loss is highly dependent upon the flow rate through the system which in turn is dependent on the pumping efficiency.

A possible design was investigated and is shown in figure 6.1.2 however a large amount of testing would need too be carried out before its performance could be

known. Due to the atmospheric conditions in the Antarctic it is important that the design be able to stand extremes of temperature and also harsh winds for long periods of time.

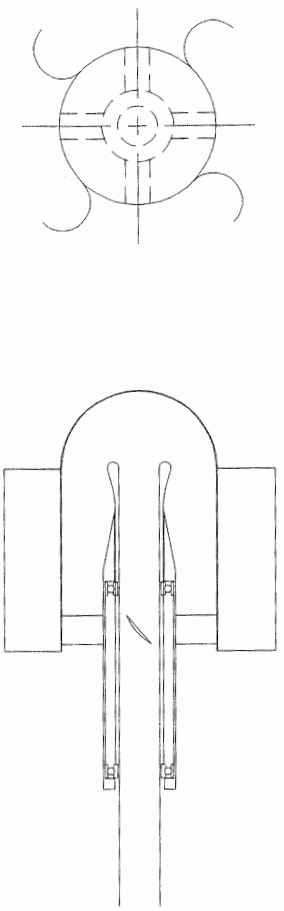

Figure 6.1.2 - alternative design to gooseneck

The design shown above would act as a wind powered turbine and use the energy harnessed to pump air through the inlet. A problem with this design is the behaviour of the flow is very difficult to predict, the pumping efficiency of the system is very difficult to determine and the flow still undergoes a 180° turn. The resistance to this is not likely to be as great as that in the original gooseneck inlet and could be further investigated. Possible problems with this design may be that it is not as robust as the

original design and that number of moving parts may make it unsuitable for the cold, icy conditions.

5.3 Alternatives to T-junction in inlet

Another part of the inlet section identified as contributing greatly to the total system losses was the T-junction, designed so to divide the flow and inject it into the chamber at opposite ends. This principle is unlikely to have a significant effect on the operation of the system, since any advantages gained by dividing the flow would be lost due to the increase in resistance. Therefore the total flow through the chamber would be decreased.

If this inlet was changed to a single pipe injecting flow into the chamber and by placing the inlet and outlet at opposite ends of the chamber the speed of flow over the samples would be effectively doubled which should significantly increase the performance of the system. The speed of the wind flow over the samples could also be improved by increasing circulation inside the chamber.

Recalculating the expected flow-rate through the system using a single entrance pipe rather than a T-junction gives a flow of 6.23 l/s. This can be compared to the previously calculated value of 5.55 l/s. This improvement is significant enough to imply that the T-junction does not improve the operation of the system.

7. CONCLUSIONS AND RECOMMENDATIONS

Preliminary testing of the venturi design was found to verify previous results in showing that the pressure distribution is axially symmetric. Further investigation showed that the optimum diffuser angle was approximately 7°, this was however a broad peak of higher efficiency therefore the exact angle was not considered important.

An inlet cylinder was attached to the venturi model and the effect on pressure distribution was found to be negligible. The flow distribution around the venturi model was also investigated and it was found that only a small fraction of the flow flowing onto the face of the venturi was passing through the throat.

The relative efficiency of the venturi-style air pump when calculated as a fraction of the energy flux onto its face was found to be very small compared to other wind powered turbines. This can be explained by the previous findings showing that most of the flow onto the inlet face of the venturi is actually diverted around the pump.

The original design of the system was designed to create a low pressure in the chamber to hasten the drying process however this proved unsuccessful. As a result of this many parts of the system should have been re-designed with consideration for a high flow-rate system.

Given that a change of angle of the diffuser from 15° to 7° dramatically increased the effectiveness of the venturi as a pump, it is suggested that should further improvements in pumping efficiency be necessary, it would be more advisable to look towards building a wind powered turbine into the design rather than to seek further improvements on the venturi-style design.

It is suggested that the venturi design used in the original model may not have been the best solution. Further study could be conducted as to whether a simple, geometrically shaped body will give a better suction coefficient than the venturi meter. The optimum design would be of the shape which produced the lowest pressure on the wall while a small amount of flow was injected into it at that point.

Another area which could be investigated is whether a more efficient venturi shaped body could be found. The dimensions of a venturi meter are shown in figure 7.1 below, the importance and effect in changing each of these dimensions could be examined. Various nozzle and diffuser shaped models, all dimensionally similar, could also be compared.

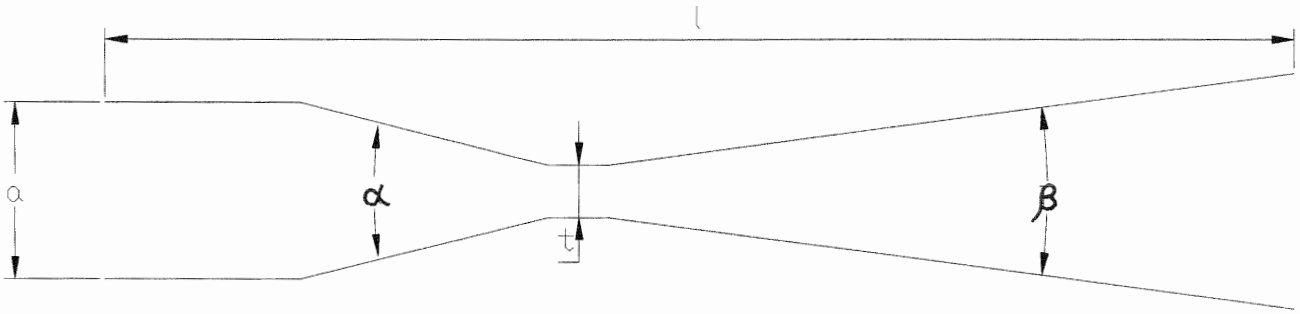

Figure 7.1 - Characteristic dimensions of a venturi

8. BIBLIOGRAPHY

[1] Akbarzadeh, A., Fundamentals of Remote Area Power Supply Systems,
Renewable Energy Authority of Victoria, Melbourne, 1992

[2] Ambrose, W.R., Application of freeze-drying to archaeological wood,
pp235 - 261 in R.M. Rowell and R.J. Barbour (eds), *Archaeological Wood: Properties Chemistry and Preservation* Advances in Chemistry Series No. 225,
American Chemical Society, 1990

[3] Ambrose, W.R., Antarctic freeze-drying of waterlogged timbers: a feasibility report,
Proceedings of the 5th ICOM Group on Wet Organic Archaeological Materials Conference, Portland/Maine, 1993

[4] Hallström, B., Skjöldebrand, C. and Trägårdh, C., Heat Transfer And Food Products,
Elsevier Applied Science, Essex, 1988

[5] Mellor, J. D., Fundamentals of Freeze Drying,
Academic Press, London, 1978

[6] Pendelbury, V., The Antarctic Freeze Drying of Waterlogged Timbers,
CM95/29, Department of Civil and Mechanical Engineering,
University of Tasmania, 1995

[7] Rae, W.H. and Pope, A., Low Speed Wind Tunnel Testing,
John Whiley & Sons. 1984

[8] Streeter, V.L. & Wylie, E.B., Fluid Mechanics,
McGraw-Hill Ryerson Limited, Singapore, 1983

[9] Twidell, John, A Guide to Small Wind Energy Conversion Systems,
Cambridge University Press, Cambridge, 1987

[10] FIDAP 7.0 Theory Manual,
Fluid Dynamics International, 1993

[11] B.S. 1042, Parts 1 and 3.

APPENDIX A

FIDAP RESULTS

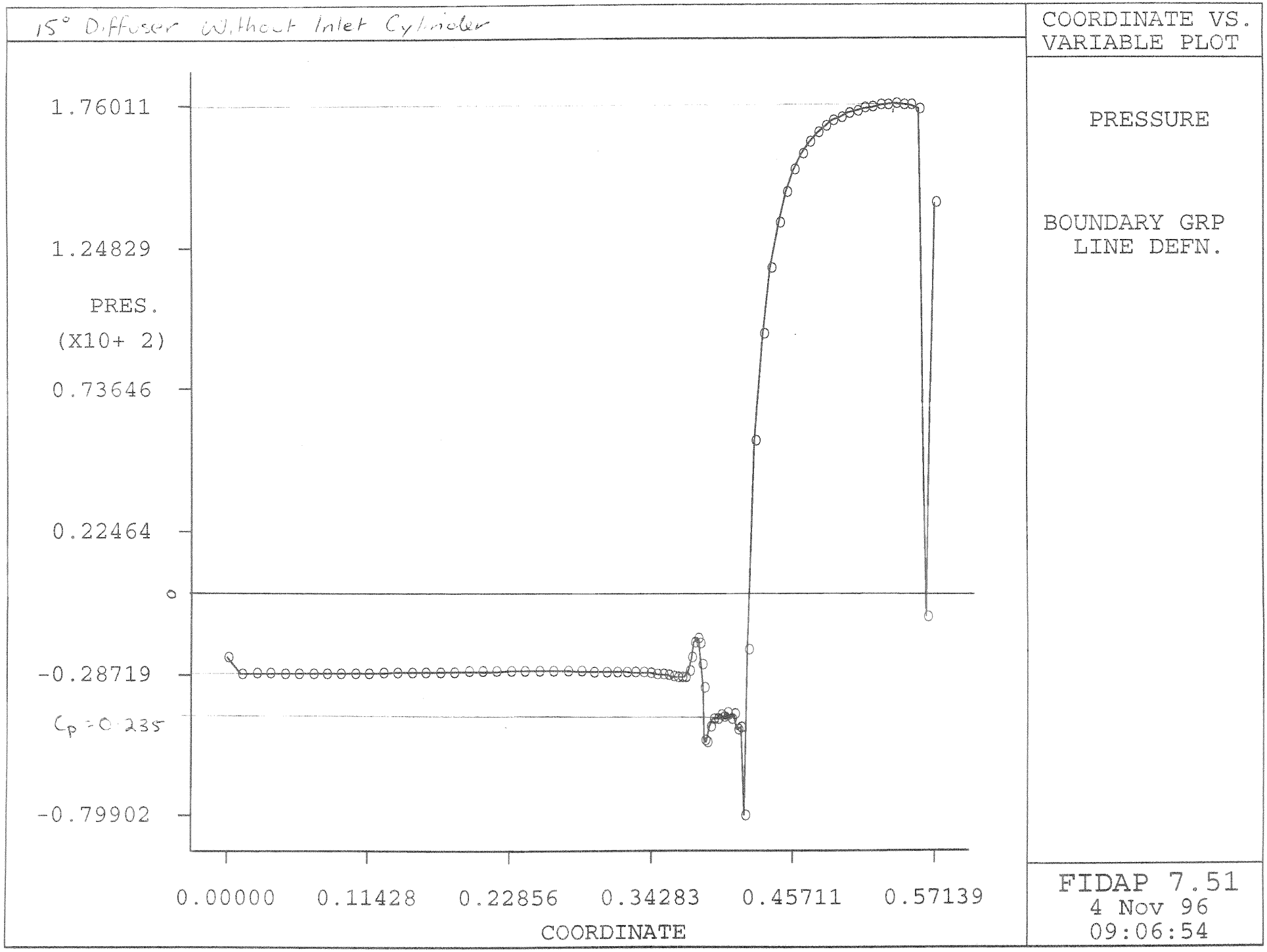
15° Diffuser Without Inlet Cylinder
COORDINATE VS. VARIABLE PLOT
PRESSURE
BOUNDARY GRP LINE DEFN.
1.76011
1.24829
PRES.
(X10+ 2)
0.73646
0.22464
0
-0.28719
$C_p = 0.235$
-0.79902
0.00000
0.11428
0.22856
0.34283
0.45711
0.57139
COORDINATE
FIDAP 7.51
4 Nov 96
09:06:54

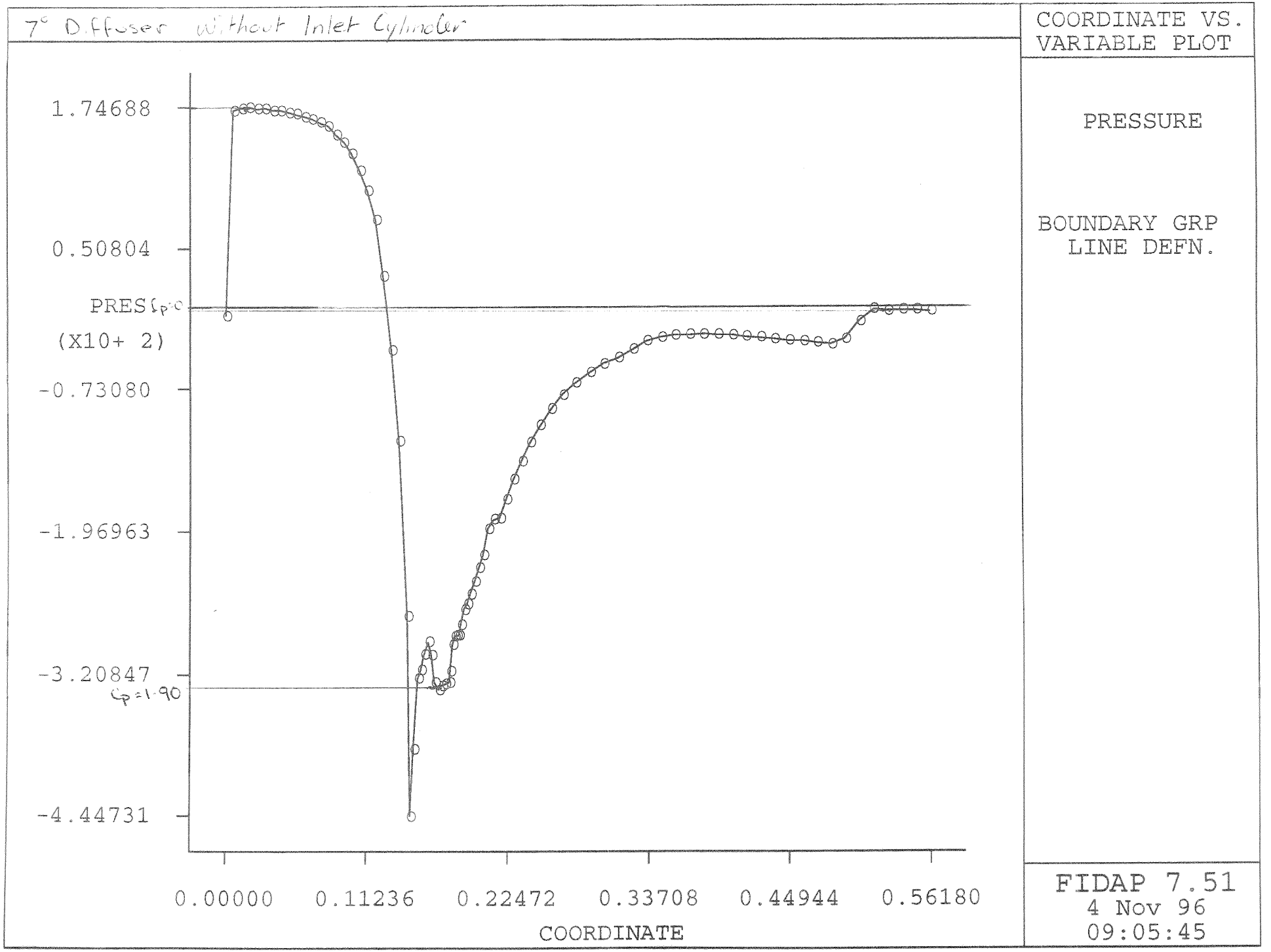
7° Diffuser without Inlet Cylinder
COORDINATE VS. VARIABLE PLOT
PRESSURE
BOUNDARY GRP LINE DEFN.
1.74688
0.50804
PRES
(X10+ 2)
-0.73080
-1.96963
-3.20847
Cp=1.90
-4.44731
0.00000
0.11236
0.22472
0.33708
0.44944
0.56180
COORDINATE
FIDAP 7.51
4 Nov 96
09:05:45

15° Diffuser With Inlet Cylinder

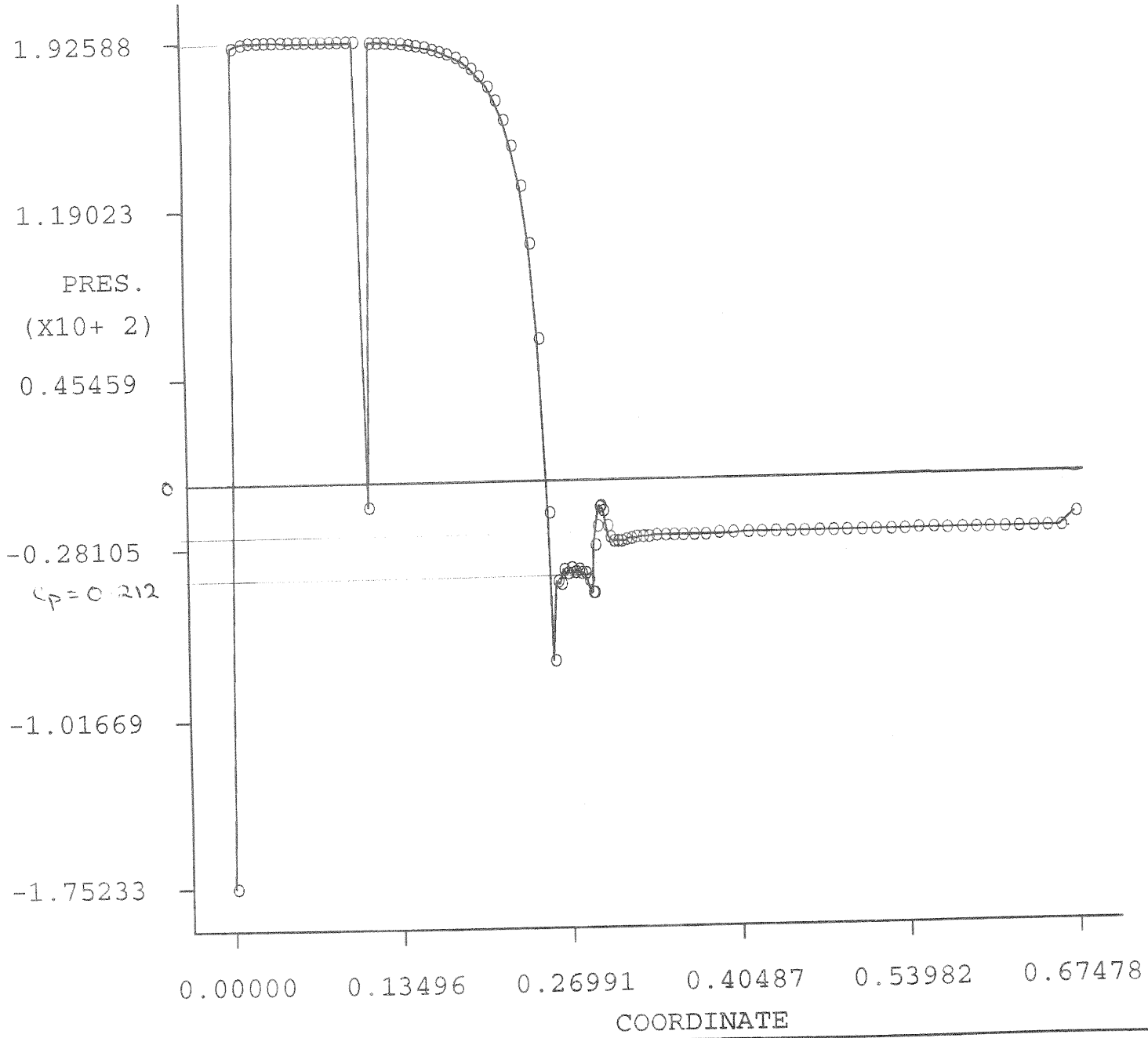

COORDINATE VS. VARIABLE PLOT

PRESSURE

BOUNDARY GRP
LINE DEFN.

FIDAP 7.51
4 Nov 96
09:01:35

7° Diffuser With Inlet cylinder

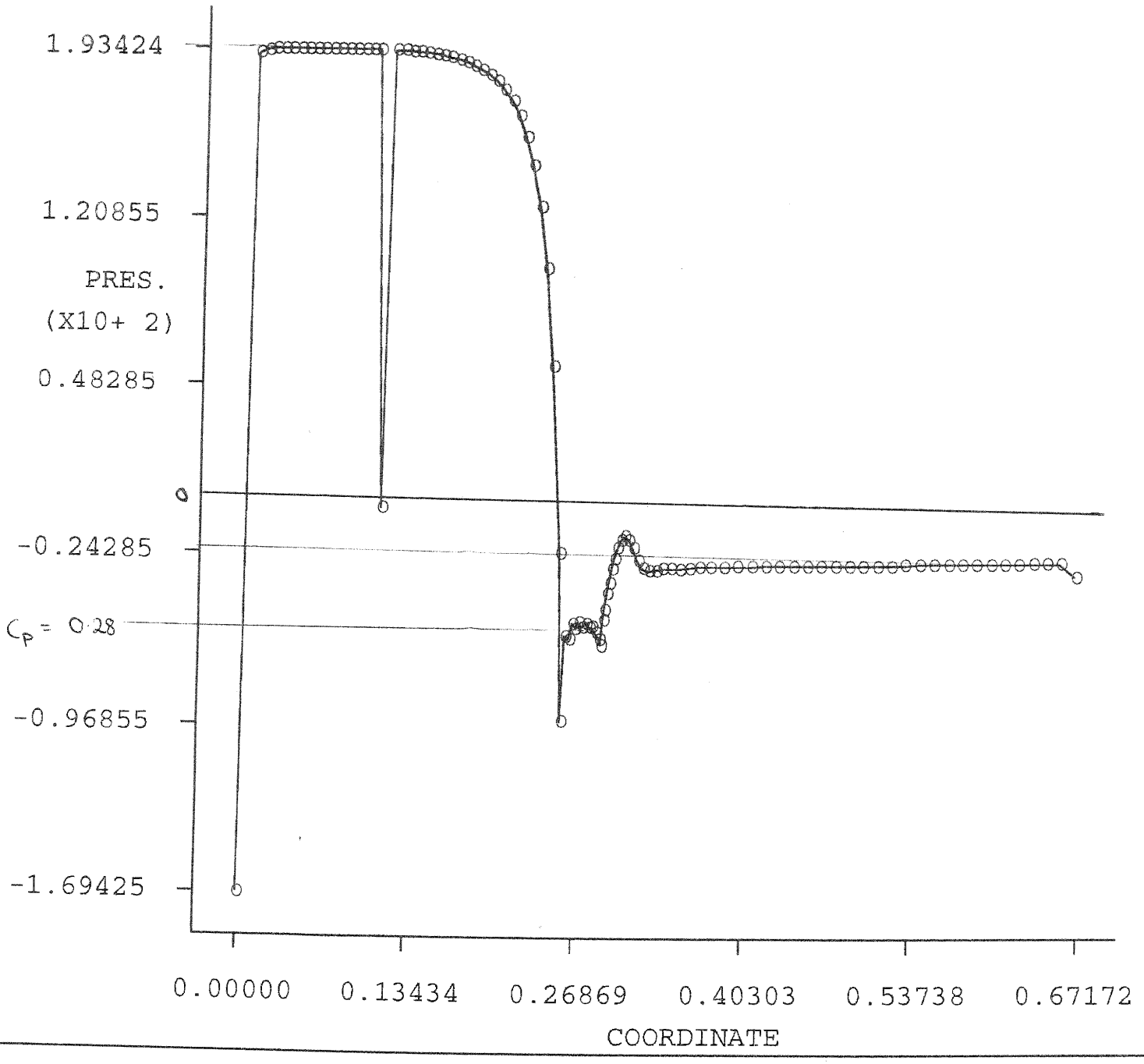

COORDINATE VS. VARIABLE PLOT

PRESSURE

BOUNDARY GRP
LINE DEFN.

FIDAP 7.51
4 Nov 96
09:02:15

15° Diffuser without Inlet Cylinder

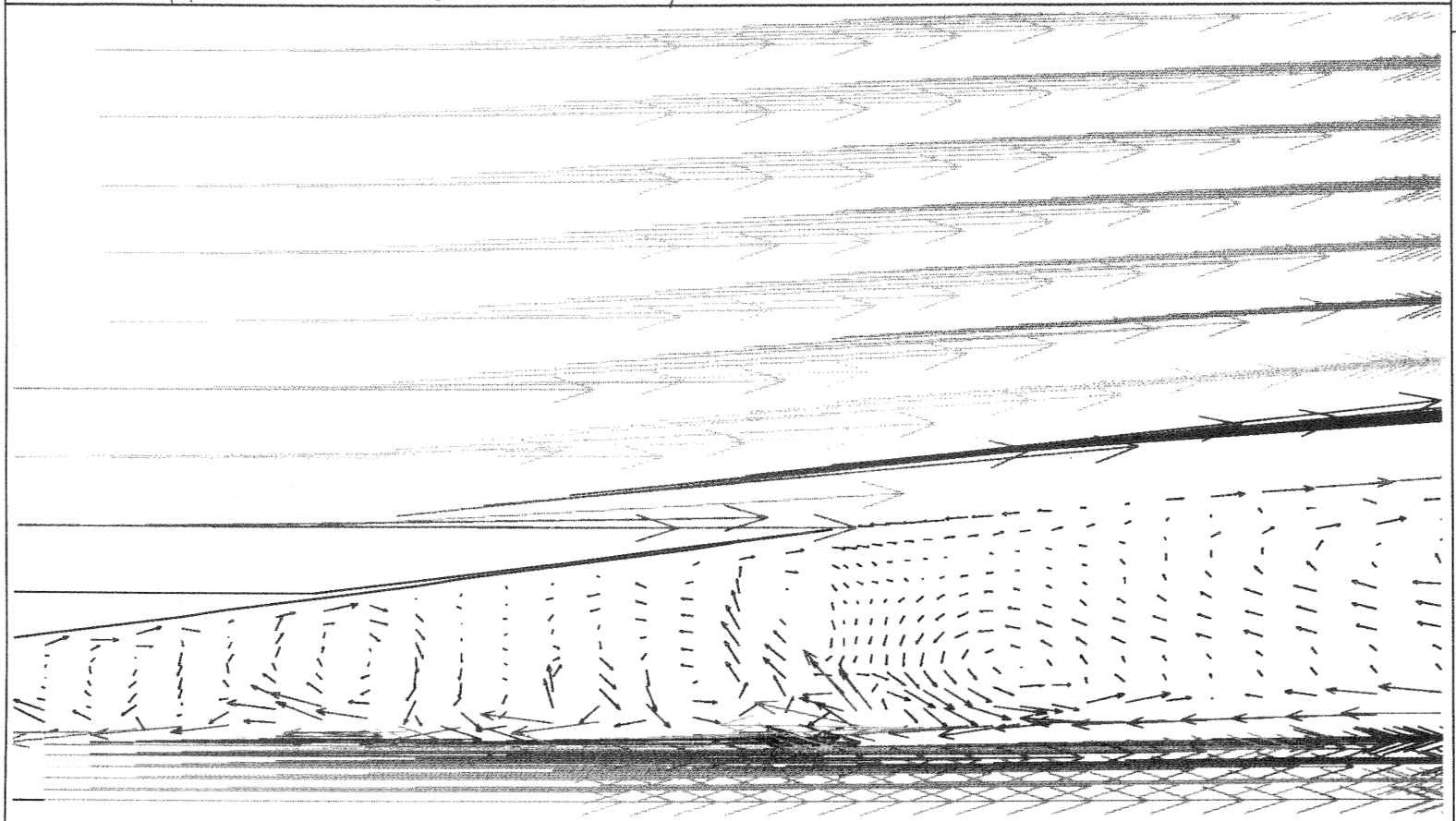

VELOCITY
VECTOR PLOT

SCALE FACTOR
0.5000E+03

REFER. VECTOR
⟶ 0.2335E+01

MAX.VEC.PLOT'D
0.2319E+02
AT NODE 3103

COLOR CODE:
VELOCITY

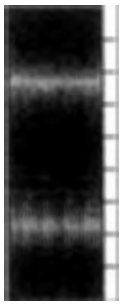

0.208E+02
0.182E+02
0.156E+02
0.130E+02
0.104E+02
0.778E+01
0.519E+01
0.259E+01

SCREEN LIMITS
ZMIN 0.467E+00
ZMAX 0.816E+00
RMIN -.117E+00
RMAX 0.193E+00

FIDAP 7.51
4 Nov 96
10:17:00

R
Z

7° Diffuser without Inlet Cylinder

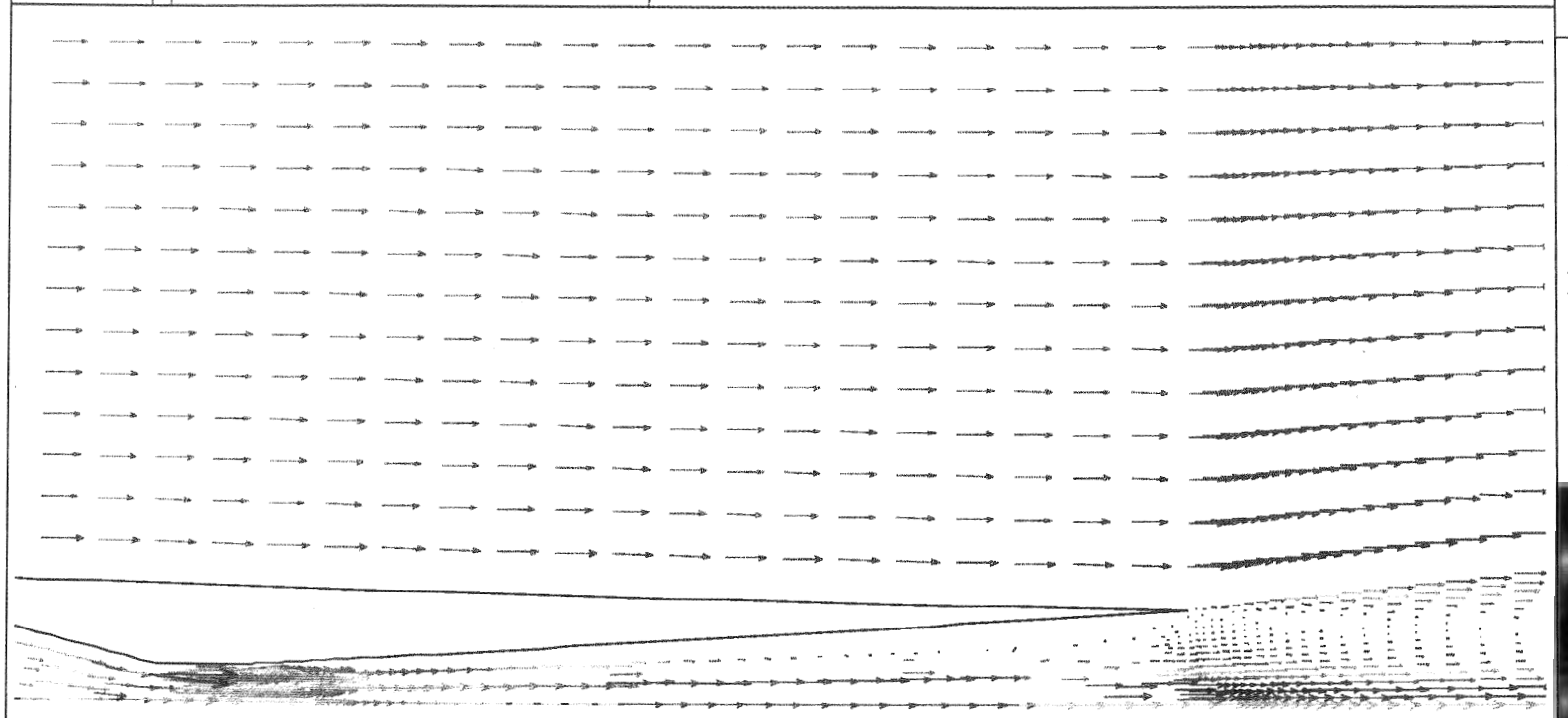

VELOCITY
VECTOR PLOT

SCALE FACTOR
0.5000E+02

REFER. VECTOR
→ 0.3877E+02

MAX.VEC.PLOT'D
0.3877E+02
AT NODE 9164

COLOR CODE:
VELOCITY

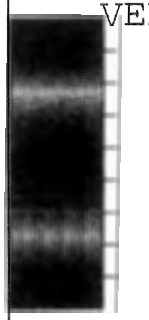

0.345E+02
0.302E+02
0.258E+02
0.215E+02
0.172E+02
0.129E+02
0.862E+01
0.431E+01

SCREEN LIMITS
ZMIN 0.192E+00
ZMAX 0.812E+00
RMIN -.272E+00
RMAX 0.277E+00

FIDAP 7.51
4 Nov 96
09:38:08

R
Z

7° Diffuser without Inlet Cylinder

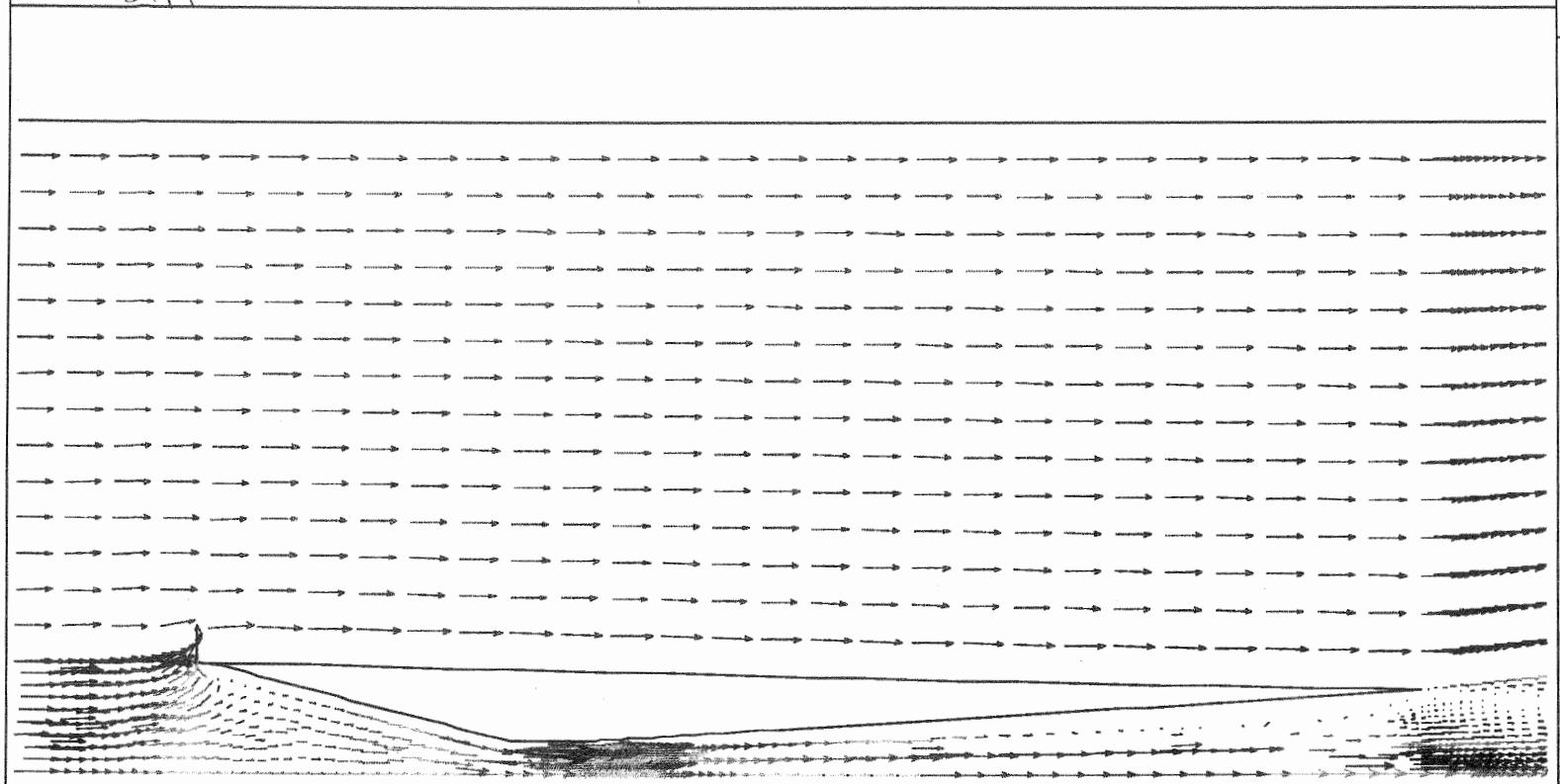

VELOCITY
VECTOR PLOT

SCALE FACTOR
0.5000E+02

REFER. VECTOR
→ 0.3877E+02

MAX.VEC.PLOT'D
0.3877E+02

AT NODE 9164

COLOR CODE:
VELOCITY

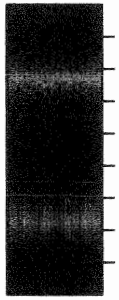

0.345E+02
0.302E+02
0.258E+02
0.215E+02
0.172E+02
0.129E+02
0.862E+01
0.431E+01

SCREEN LIMITS
ZMIN 0.214E-01
ZMAX 0.725E+00
RMIN -.276E+00
RMAX 0.348E+00

FIDAP 7.51
4 Nov 96
09:35:10

R
Z

7° Diffuser with Inlet Cylinder

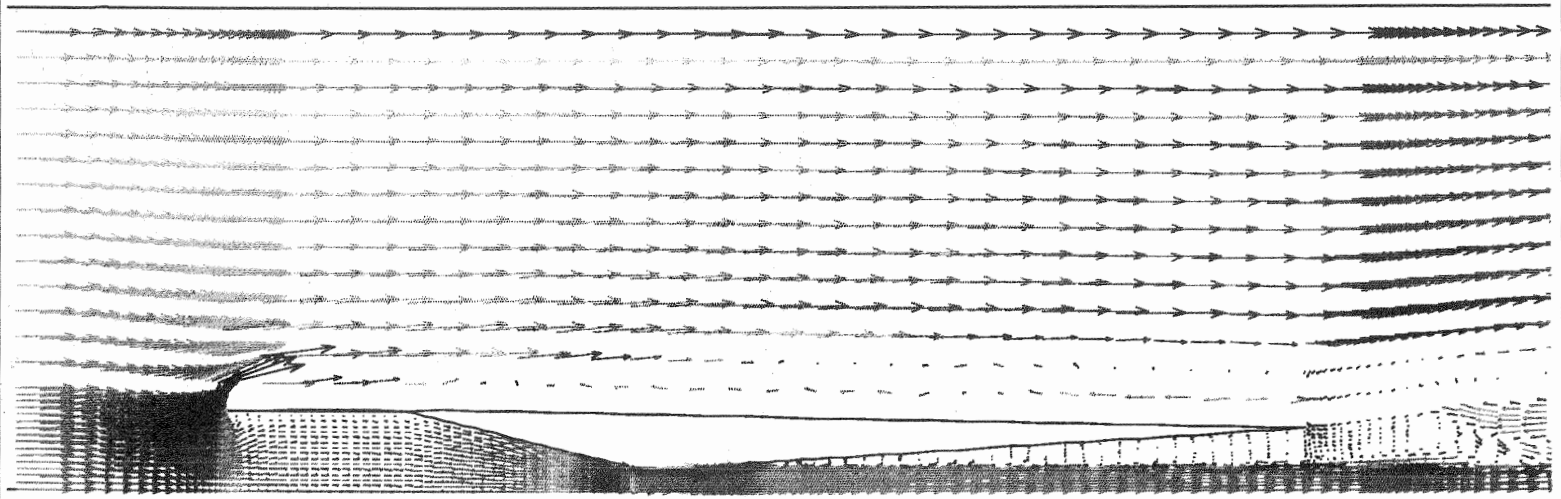

VELOCITY
VECTOR PLOT

SCALE FACTOR
0.5000E+02

REFER. VECTOR
→ 0.2407E+02

MAX.VEC.PLOT'D
0.2407E+02

AT NODE 7336

COLOR CODE:
VELOCITY

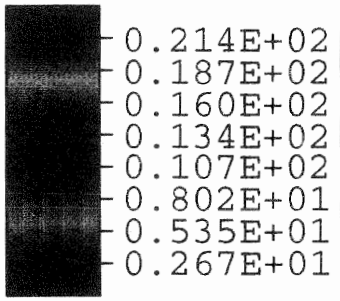

SCREEN LIMITS
ZMIN -.139E+00
ZMAX 0.819E+00
RMIN -.408E+00
RMAX 0.441E+00

FIDAP 7.51
4 Nov 96
09:32:53

R
Z

15° Diffuser Without Inlet Cylinder

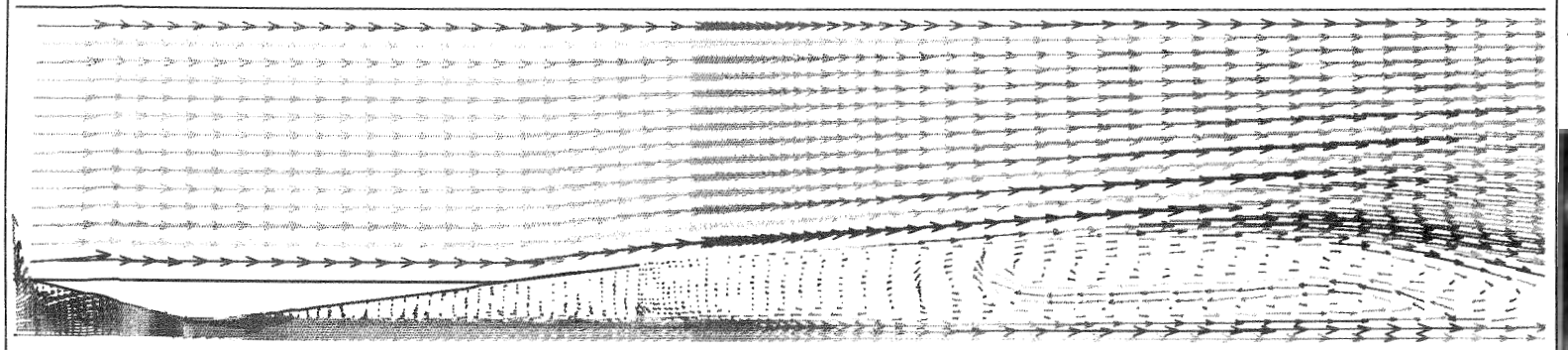

VELOCITY
VECTOR PLOT

SCALE FACTOR
0.5000E+02

REFER. VECTOR
⟶ 0.2335E+02

MAX.VEC.PLOT'D
0.2335E+02
AT NODE 3106

COLOR CODE:
VELOCITY

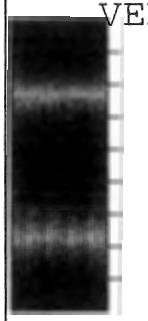

0.208E+02
0.182E+02
0.156E+02
0.130E+02
0.104E+02
0.778E+01
0.519E+01
0.259E+01

SCREEN LIMITS
ZMIN 0.930E-01
ZMAX 0.149E+01
RMIN -.625E+00
RMAX 0.617E+00

FIDAP 7.51
4 Nov 96
09:29:55

R
Z

15° Diffuser Without Inlet Cylinder

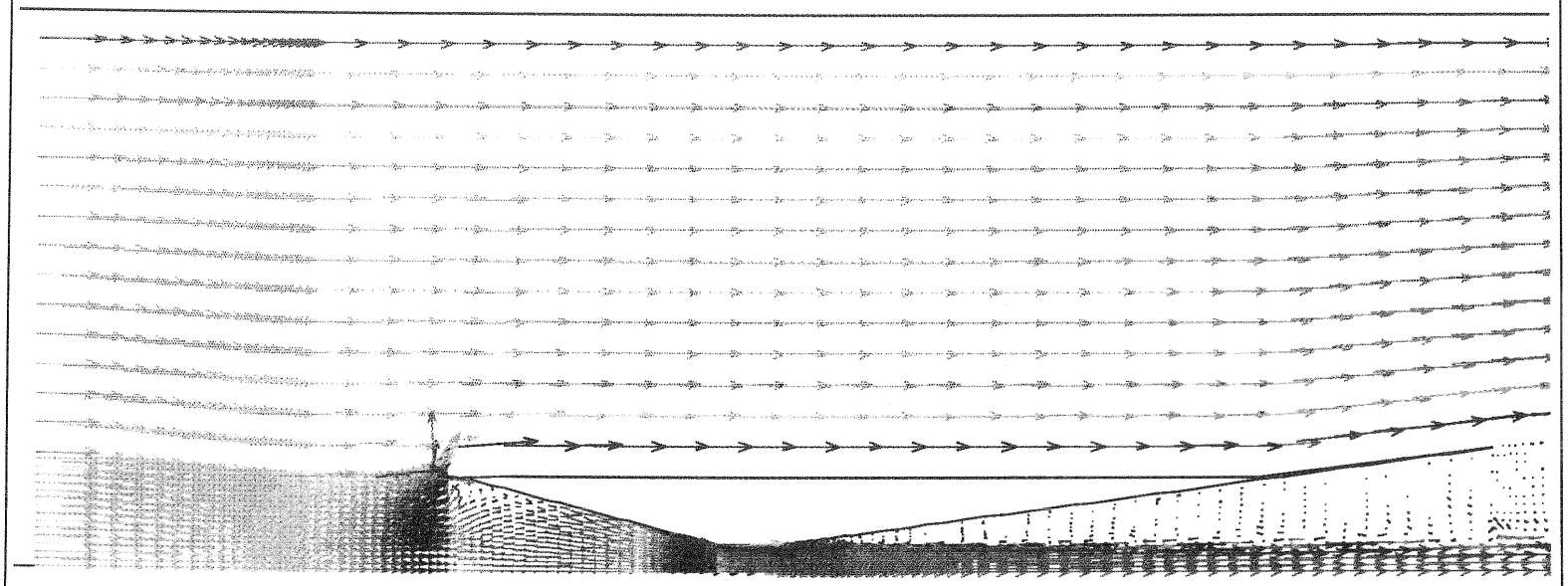

VELOCITY
VECTOR PLOT

SCALE FACTOR
0.5000E+02

REFER. VECTOR
→ 0.2335E+02

MAX.VEC.PLOT'D
0.2320E+02

AT NODE 5367

COLOR CODE:
VELOCITY

SCREEN LIMITS
ZMIN -.130E+00
ZMAX 0.699E+00
RMIN -.333E+00
RMAX 0.402E+00

FIDAP 7.51
4 Nov 96
09:24:42

R
Z

15° Diffuser With Inlet Cylinder

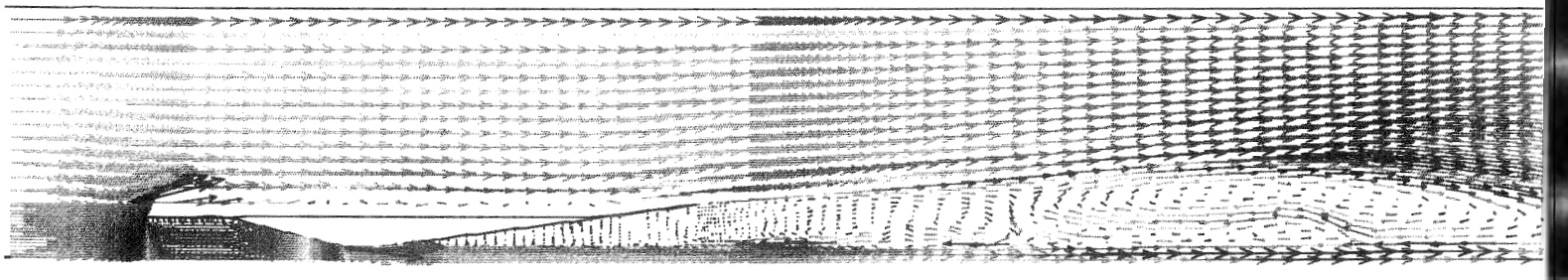

VELOCITY
VECTOR PLOT

SCALE FACTOR
0.5000E+02

REFER. VECTOR
⟶ 0.2413E+02

MAX.VEC.PLOT'D
0.2413E+02
AT NODE 1734

COLOR CODE:
VELOCITY

0.215E+02
0.188E+02
0.161E+02
0.134E+02
0.107E+02
0.804E+01
0.536E+01
0.268E+01

SCREEN LIMITS
ZMIN -.157E+00
ZMAX 0.167E+01
RMIN -.759E+00
RMAX 0.861E+00

FIDAP 7.51
4 Nov 96
09:22:07

R
Z

15° Diffuser With Inlet Cylinder

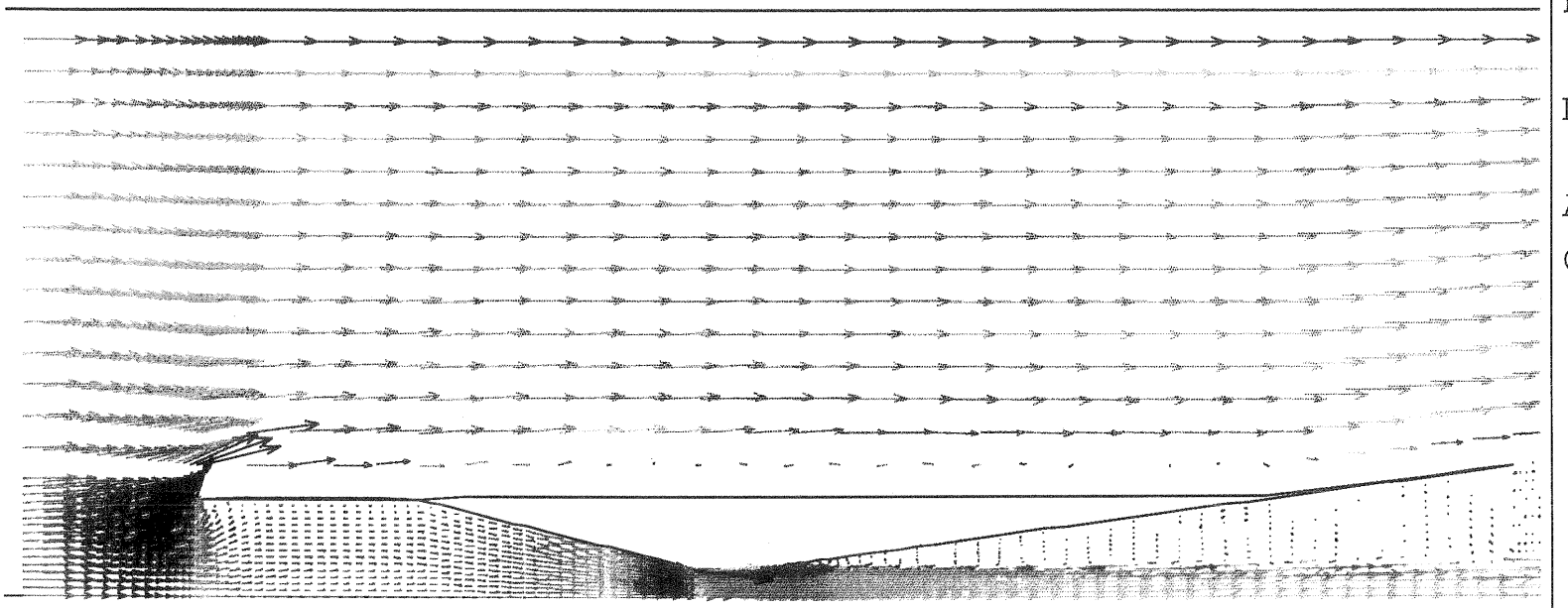

VELOCITY
VECTOR PLOT

SCALE FACTOR
0.5000E+02

REFER. VECTOR
⟶ 0.2413E+02

MAX.VEC.PLOT'D
0.2413E+02
AT NODE 1734

COLOR CODE:
VELOCITY

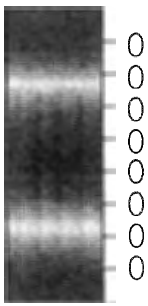

SCREEN LIMITS
ZMIN -.102E+00
ZMAX 0.681E+00
RMIN -.310E+00
RMAX 0.384E+00

FIDAP 7.51
4 Nov 96
09:20:09

R
Z

APPENDIX B

EXPERIMANTAL RESULTS

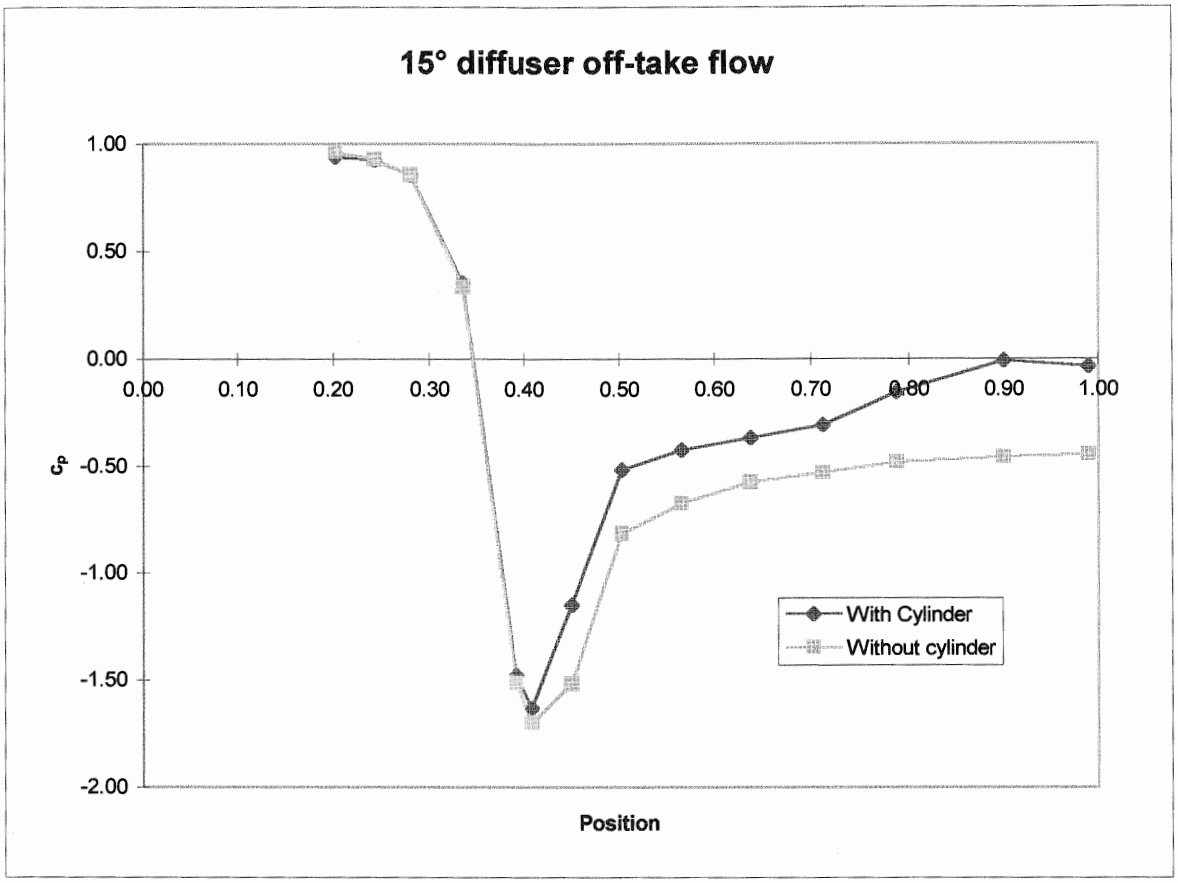
15° diffuser off-take flow
1.00
0.50
0.00
-0.50
-1.00
-1.50
-2.00
0.00
0.10
0.20
0.30
0.40
0.50
0.60
0.70
0.80
0.90
1.00
Cp
Position
With Cylinder
Without cylinder

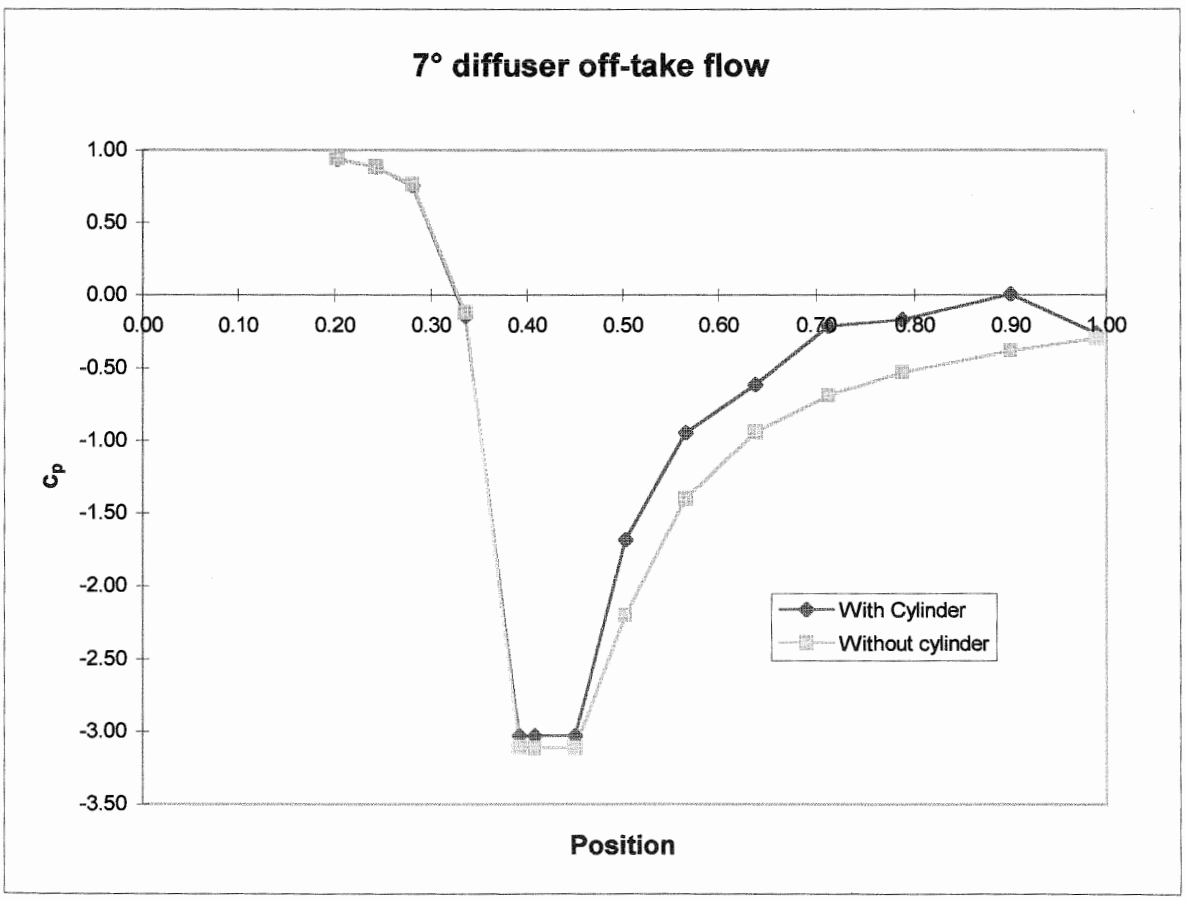
7° diffuser off-take flow
1.00
0.50
0.00
-0.50
-1.00
-1.50
-2.00
-2.50
-3.00
-3.50
0.00
0.10
0.20
0.30
0.40
0.50
0.60
0.70
0.80
0.90
1.00
Cp
Position
With Cylinder
Without cylinder

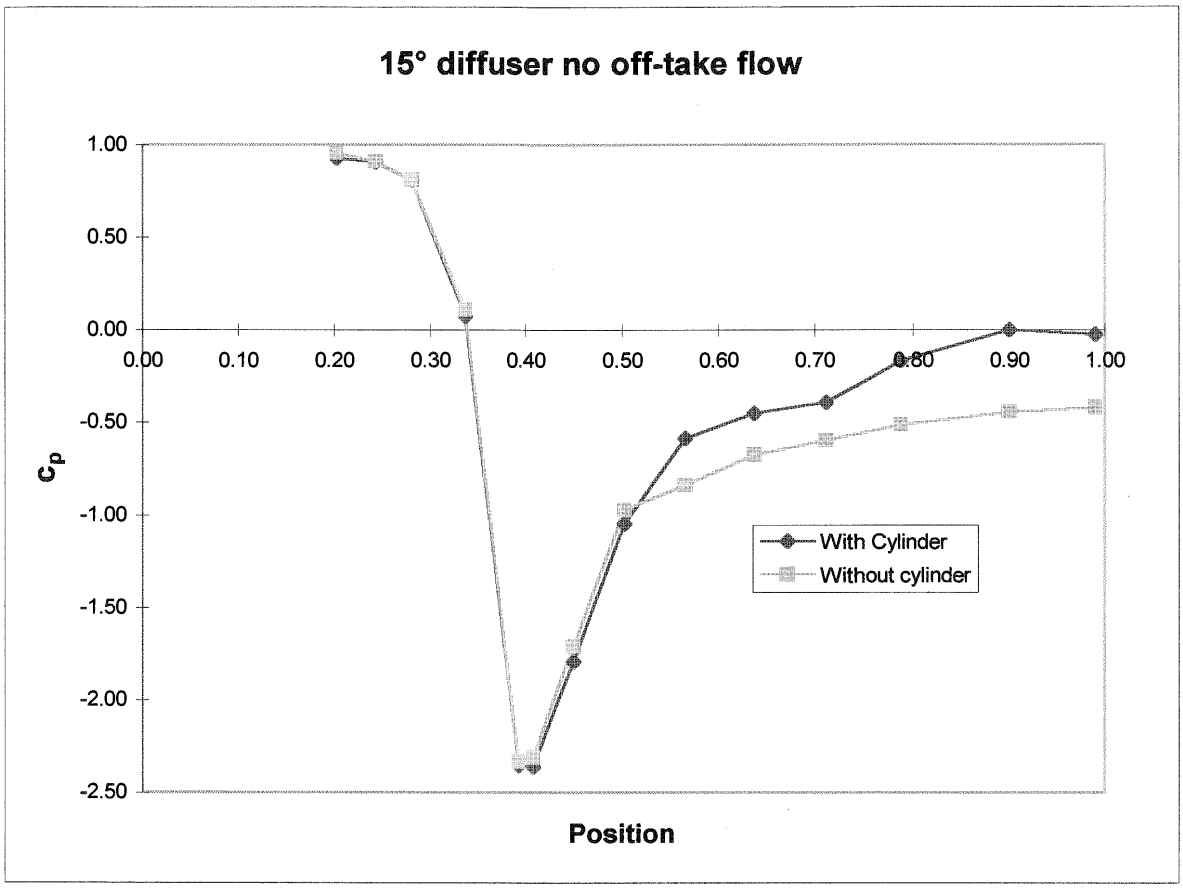
15° diffuser no off-take flow
1.00
0.50
0.00
-0.50
-1.00
-1.50
-2.00
-2.50
0.00
0.10
0.20
0.30
0.40
0.50
0.60
0.70
0.80
0.90
1.00
Cp
Position
With Cylinder
Without cylinder

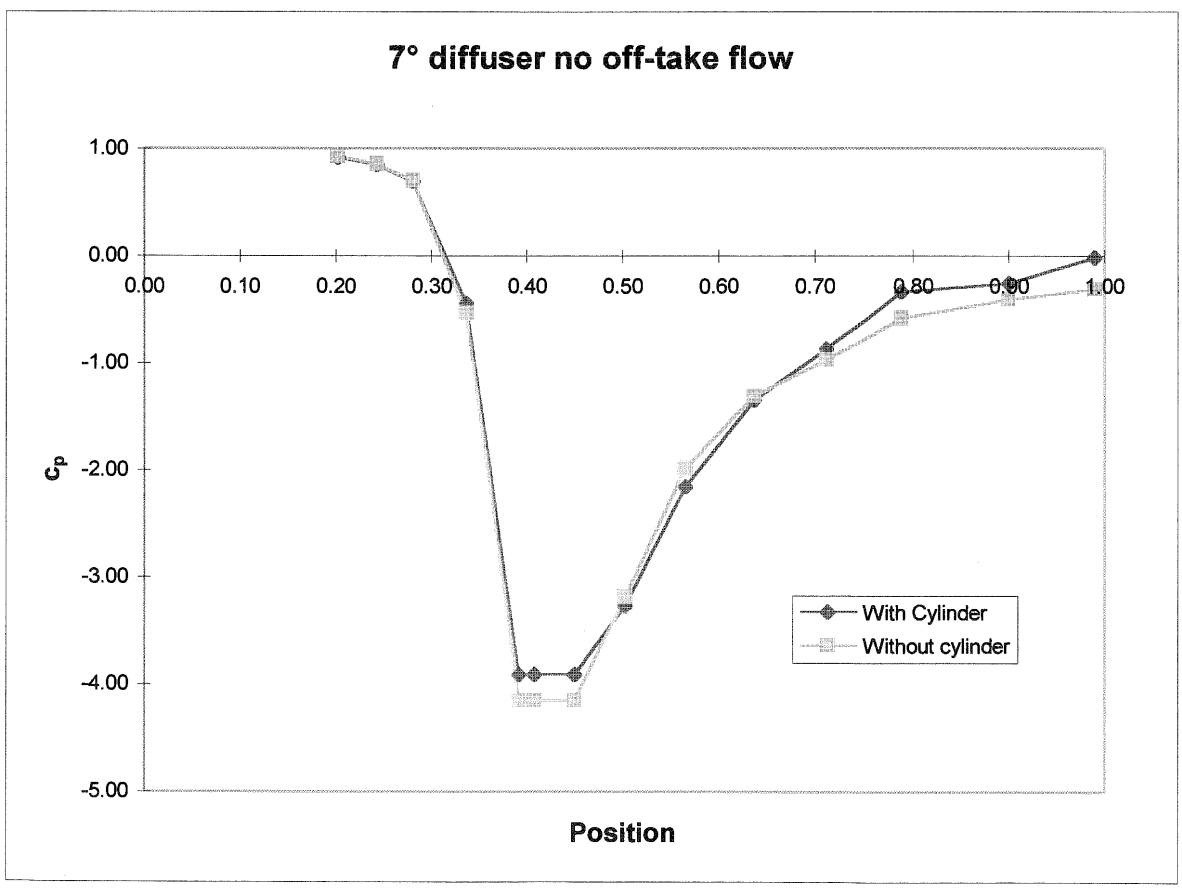
7° diffuser no off-take flow
1.00
0.00
-1.00
-2.00
-3.00
-4.00
-5.00
0.00
0.10
0.20
0.30
0.40
0.50
0.60
0.70
0.80
0.90
1.00
Cp
Position
With Cylinder
Without cylinder

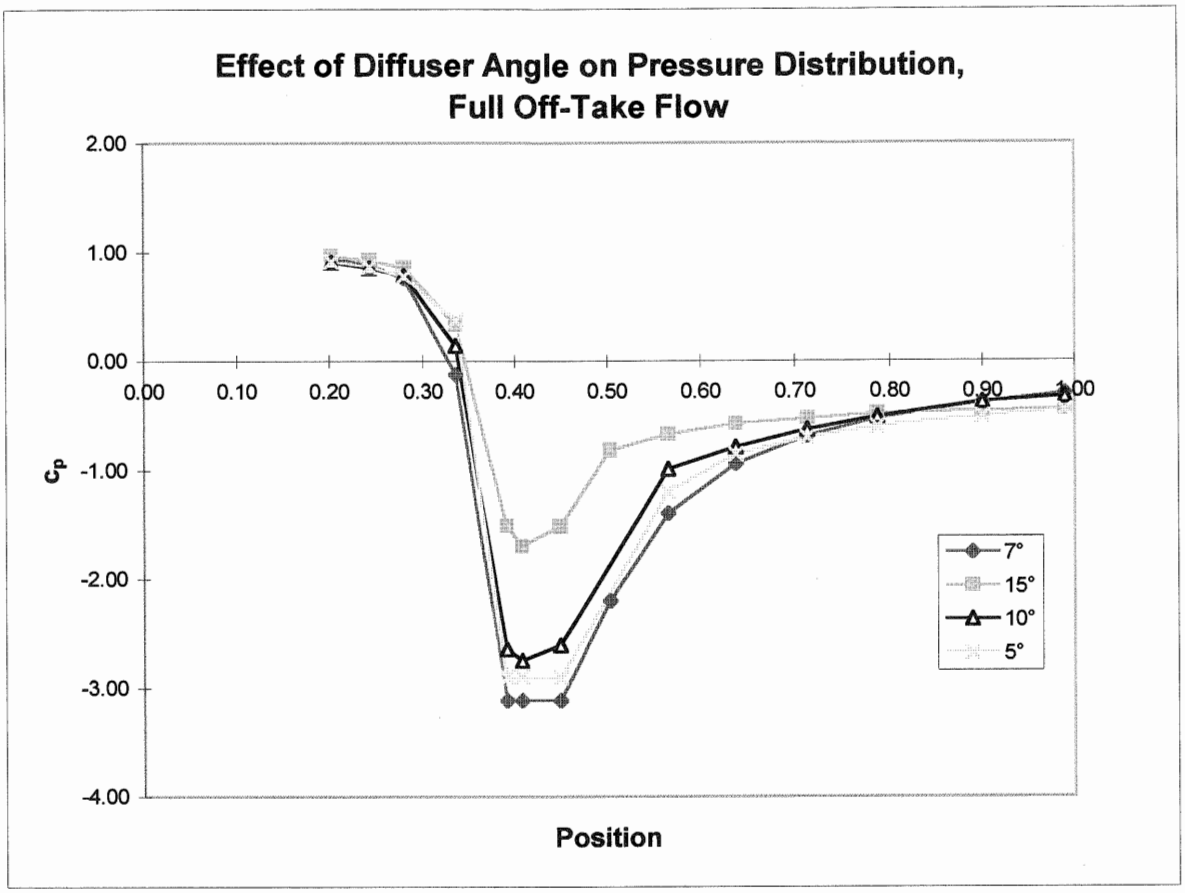
Effect of Diffuser Angle on Pressure Distribution,
Full Off-Take Flow
2.00
1.00
0.00
-1.00
-2.00
-3.00
-4.00
0.00
0.10
0.20
0.30
0.40
0.50
0.60
0.70
0.80
0.90
1.00
Cp
Position
7°
15°
10°
5°

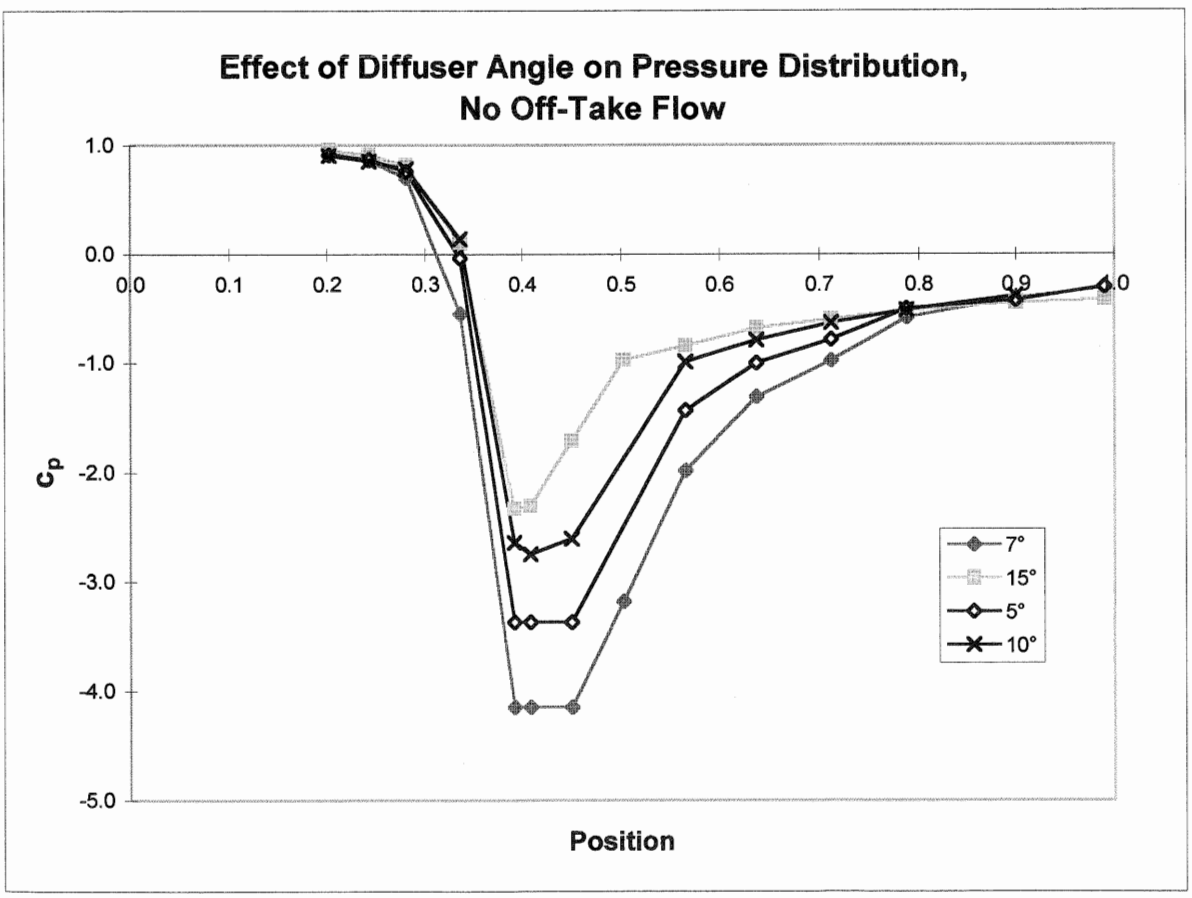
Effect of Diffuser Angle on Pressure Distribution,
No Off-Take Flow
1.0
0.0
-1.0
-2.0
-3.0
-4.0
-5.0
0.0
0.1
0.2
0.3
0.4
0.5
0.6
0.7
0.8
0.9
1.0
Cp
Position
7°
15°
5°
10°

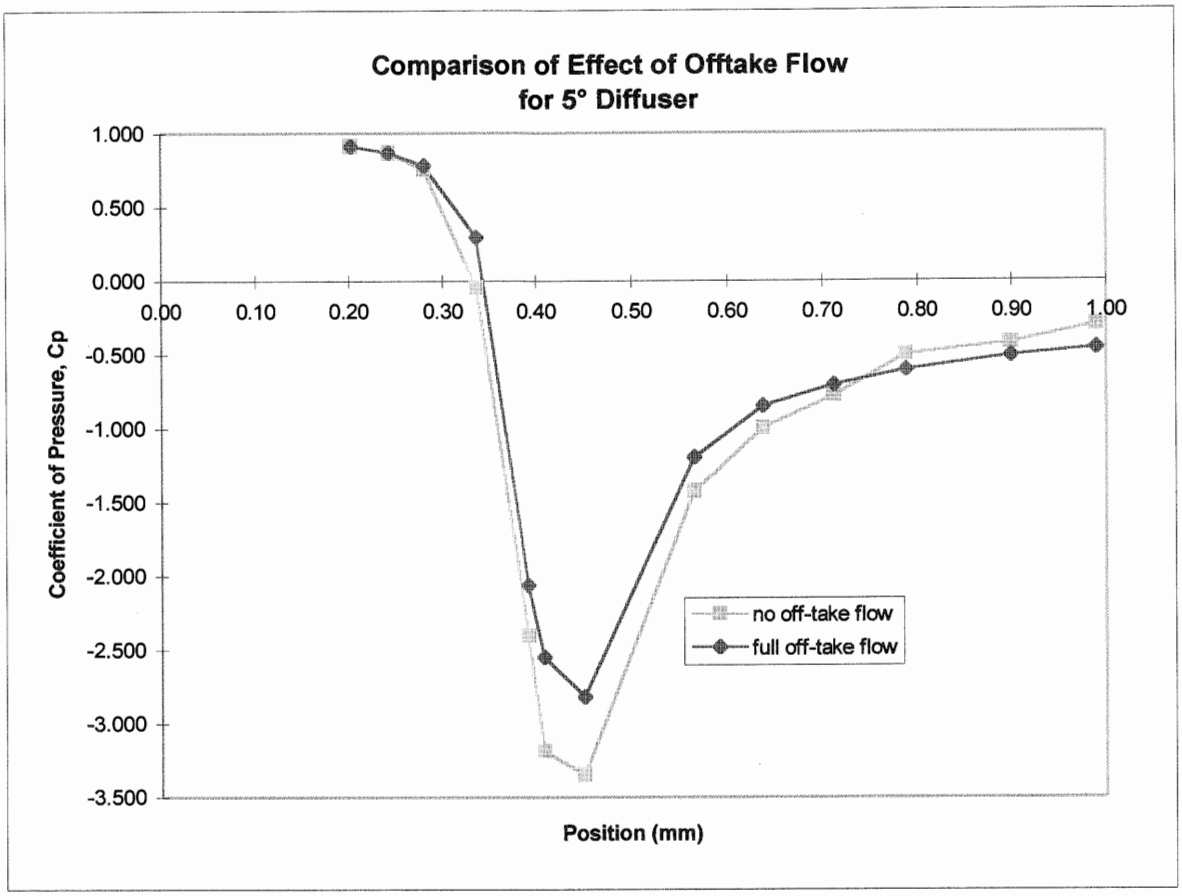
Comparison of Effect of Offtake Flow
for 5° Diffuser
Coefficient of Pressure, Cp
Position (mm)
1.000
0.500
0.000
-0.500
-1.000
-1.500
-2.000
-2.500
-3.000
-3.500
0.00
0.10
0.20
0.30
0.40
0.50
0.60
0.70
0.80
0.90
1.00
no off-take flow
full off-take flow

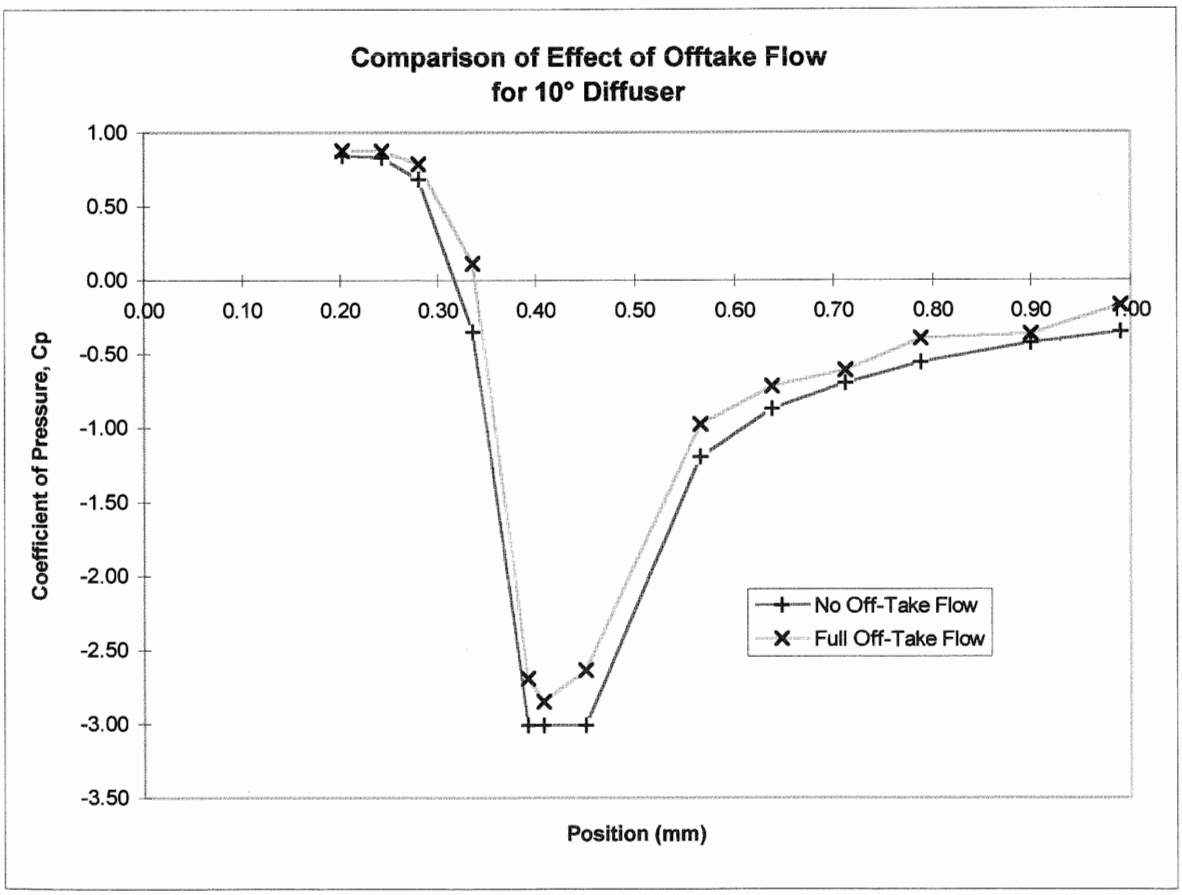
Comparison of Effect of Offtake Flow
for 10° Diffuser
Coefficient of Pressure, Cp
Position (mm)
1.00
0.50
0.00
-0.50
-1.00
-1.50
-2.00
-2.50
-3.00
-3.50
0.00
0.10
0.20
0.30
0.40
0.50
0.60
0.70
0.80
0.90
1.00
No Off-Take Flow
Full Off-Take Flow

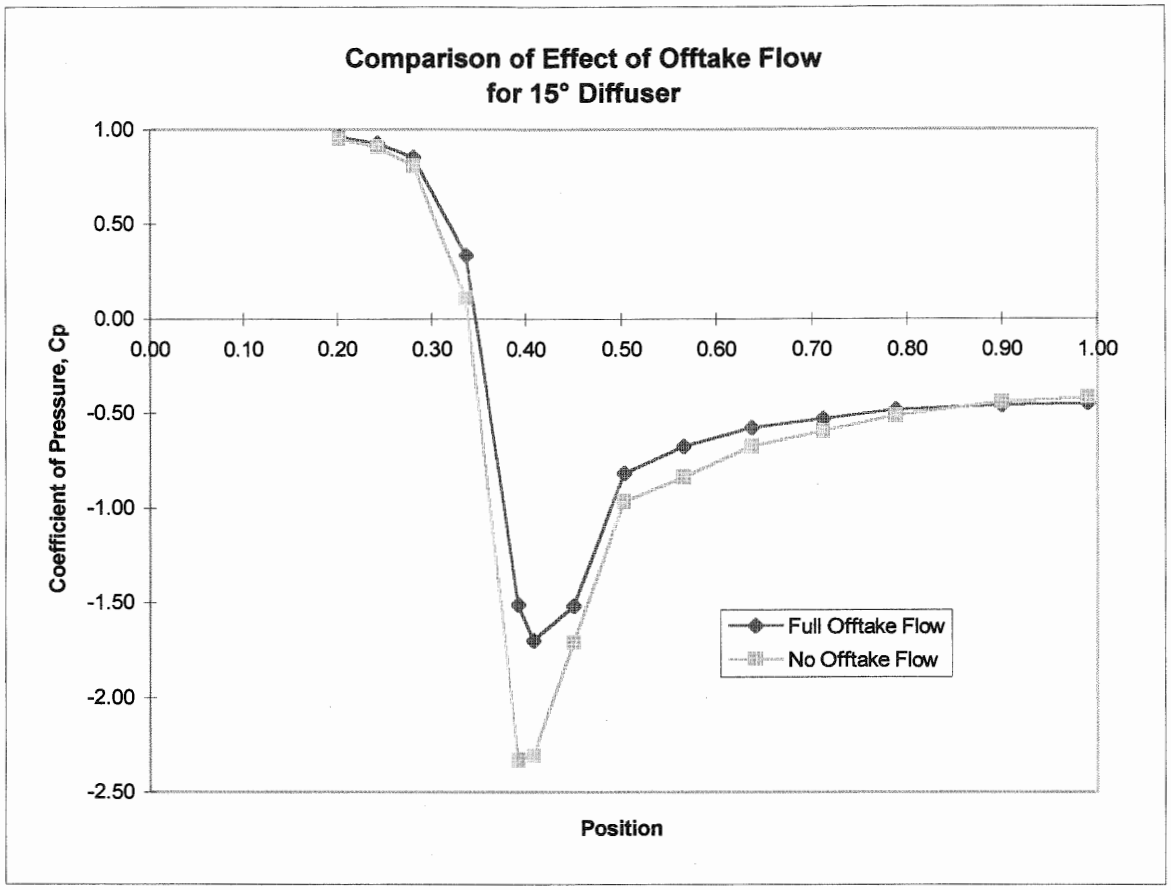
Comparison of Effect of Offtake Flow
for 15° Diffuser
Coefficient of Pressure, Cp
Position
1.00
0.50
0.00
-0.50
-1.00
-1.50
-2.00
-2.50
0.00
0.10
0.20
0.30
0.40
0.50
0.60
0.70
0.80
0.90
1.00
Full Offtake Flow
No Offtake Flow

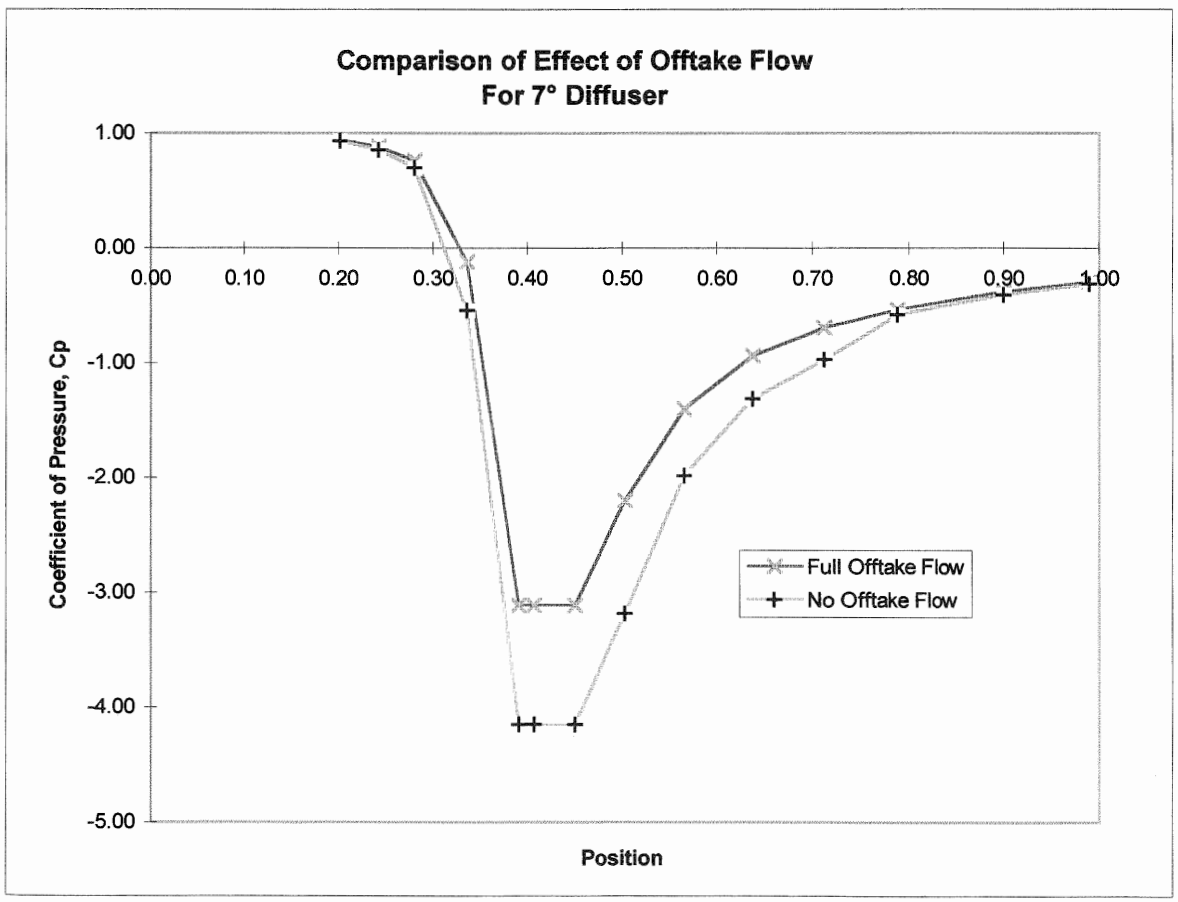
Comparison of Effect of Offtake Flow
For 7° Diffuser
Coefficient of Pressure, Cp
Position
1.00
0.00
-1.00
-2.00
-3.00
-4.00
-5.00
0.00
0.10
0.20
0.30
0.40
0.50
0.60
0.70
0.80
0.90
1.00
Full Offtake Flow
No Offtake Flow

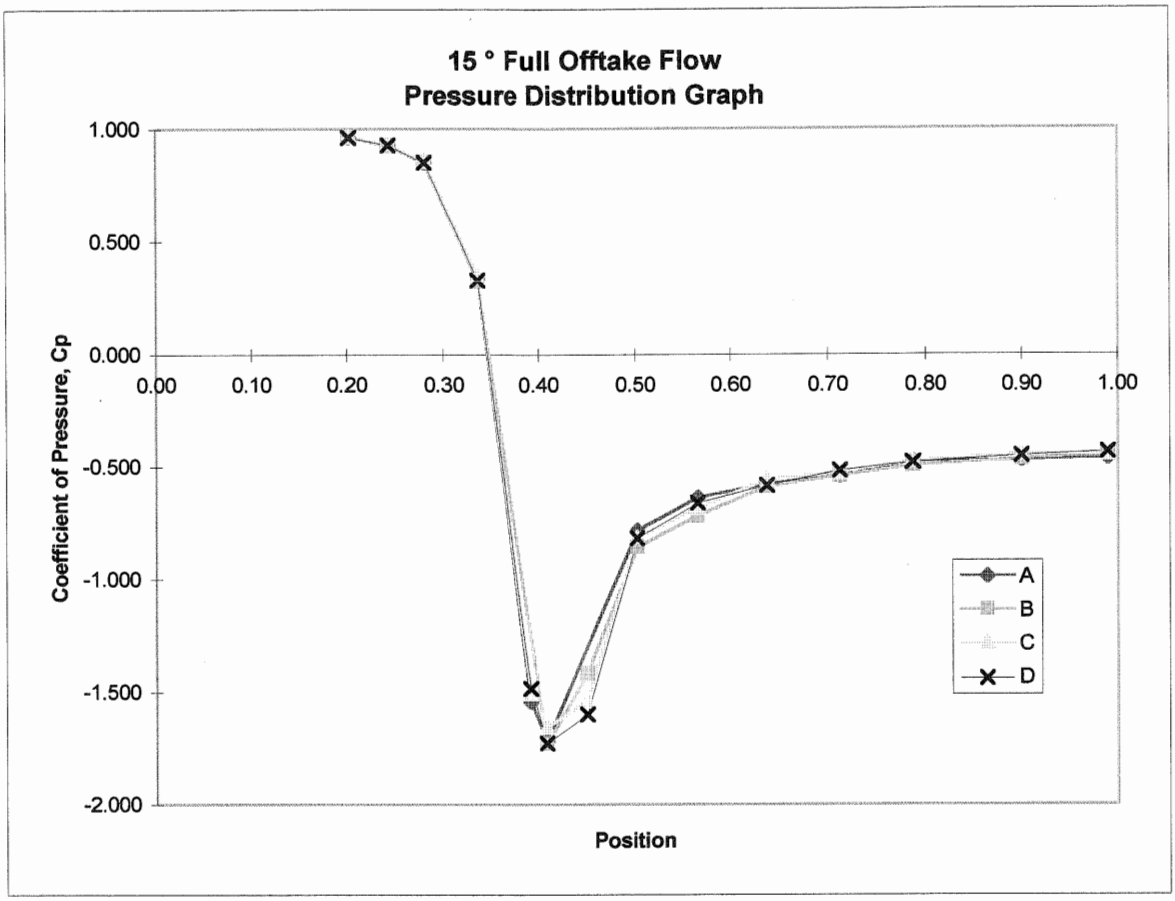
15 ° Full Offtake Flow
Pressure Distribution Graph
Coefficient of Pressure, Cp
1.000
0.500
0.000
-0.500
-1.000
-1.500
-2.000
0.00
0.10
0.20
0.30
0.40
0.50
0.60
0.70
0.80
0.90
1.00
Position
A
B
C
D

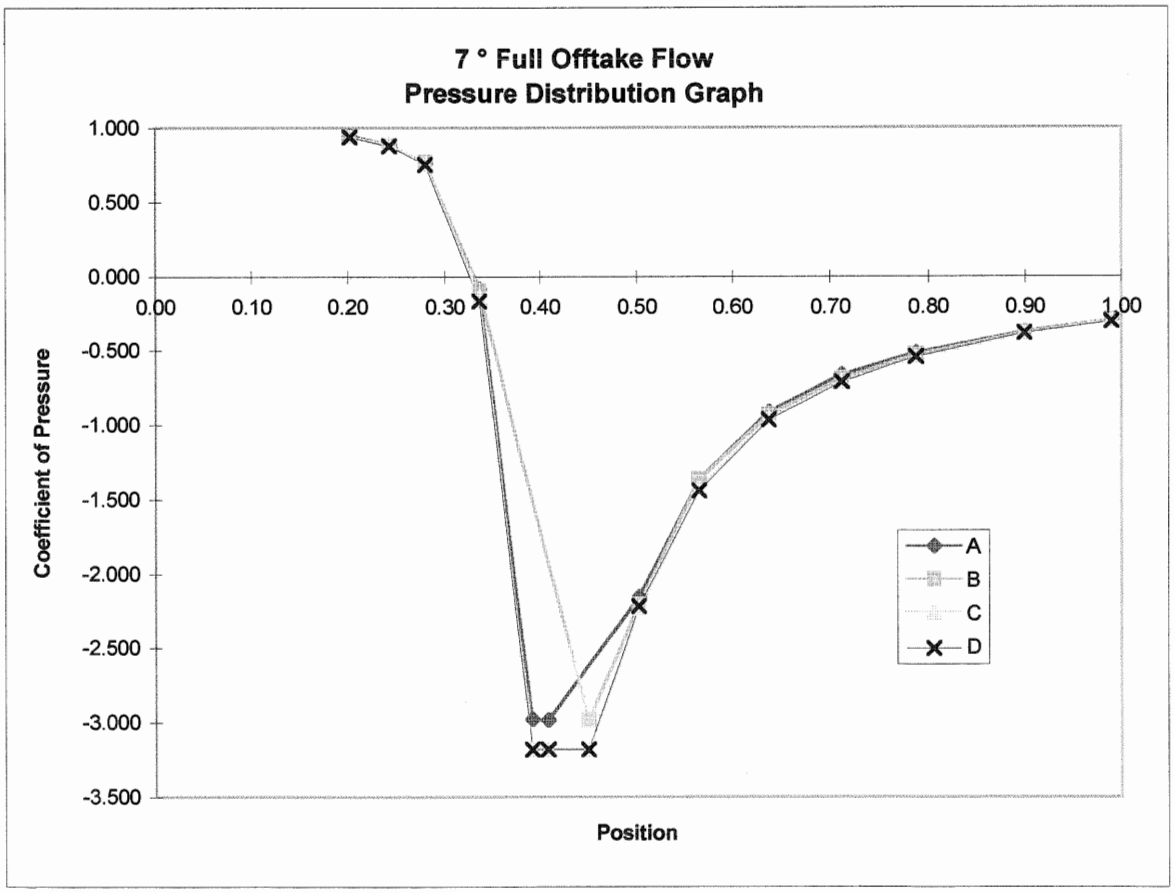
7 ° Full Offtake Flow
Pressure Distribution Graph
Coefficient of Pressure
1.000
0.500
0.000
-0.500
-1.000
-1.500
-2.000
-2.500
-3.000
-3.500
0.00
0.10
0.20
0.30
0.40
0.50
0.60
0.70
0.80
0.90
1.00
Position
A
B
C
D

APPENDIX C

THEORY OF HEAT TRANSFER

APPENDIX C

Heat Transfer Equation for Atmospheric Freeze Drying

We can use the boundary conditions at the interface:

$$\rho_i \Delta H\left(m_0 + m_f\right)\frac{\partial X}{\partial t} = -\lambda_d\left(\frac{\partial X}{\partial t}\right)_{x=X} + \lambda_i\left(\frac{\partial T_i}{\partial x}\right)_{x=X} \qquad \text{eq. C.1}$$

where

m_0 = initial moisture content of dry basis

m_f = final moisture content of dry basis

λ_i = thermal conductivity of ice

T_i = ice temperature

X subscript $\Rightarrow$ interface

Since we know the temperature of the ice is a function of both position and time we can write:

$$\lambda_i\left(\frac{\partial T_i}{\partial x}\right)_{x=X} = \lambda_i\left\{\frac{\partial T_i}{\partial t}\left(\frac{\partial t}{\partial x}\right)_{x=X} + \frac{\partial T_i}{\partial x}\left(\frac{\partial x}{\partial x}\right)_{x=X}\right\}$$

we know that the temperature gradient, $\frac{\partial T_i}{\partial x}$, in the ice is very small thus we can neglect the second term, we also know that by definition,

$X\left(\frac{\partial x}{\partial t}\right)_{x=X} = \frac{\lambda_i}{c_i \rho_i (1+m_0)}$, this gives us:

$$\lambda_i \frac{\partial T_i}{\partial x} = \rho_i X (1+m_0) c_i \frac{\partial T_i}{\partial t}$$

therefore substituting into eq. C.1 we get:

$$\rho_i \Delta H (m_0 - m_f) \frac{dX}{dt} = -\lambda_d \left(\frac{\partial T}{\partial x}\right)_{x=X} + \rho_i X c_i (1+m_0) \frac{\partial T_i}{\partial t}$$

where c_i = specific heat of ice

APPENDIX D

CALCULATION OF OFF-TAKE FLOW RATE

APPENDIX D

Calculation of Off-take Flow Rate

The volumetric flow-rate through a bellmouth nozzle is given by:

$$Q = C_{DN} \frac{\pi d_n^4}{4} \sqrt{\frac{2\Delta p_b}{\rho(1-m)^2}}$$

where $\sqrt{m}$ is the ratio of the downstream nozzle diameter to the upstream diameter, here the upstream diameter is effectively infinite therefore it can be assumed that m=0. The equation then simplifies to:

$$Q = C_{DN} A_o \sqrt{\frac{2\Delta p_b}{\rho}}$$

where C_{DN}= C(m).Z(Rd,m).Z(d,m).ε which are obtained from BS 1042

Sample Off-take Flow Calculation:

Calculation of off-take flow rate for 7° diffuser

Temperature = 21.8 °C

Humidity = 45.5 %

Barometric Pressure = 1000.7 Pa

Δp measured = 336.26 Pa

Now $A_0 = \frac{\pi d_n^2}{4} = \frac{\pi \times 0.008^2}{4} = 5.027 \times 10^{-5}$

ρ = 1.176 from psychrometric chart

from BS 1042 (relevant sections)

81 e: C = 0.987

81 g: $Z_D = 1$

81 h: ε=1 (for a incompressible fluid)

it is assumed that R_d=20 000 thus Z_R=0.96

thus $C_{DN} = C.Z_D.Z_R.\varepsilon = 0.987*1*1*0.96 = 0.948$

$$Q = 0.948 \times 5.027 \times 10^{-5} \times \sqrt{\frac{2 \times 336.26}{1.176}} = 1.1390 \times 10^{-3} \quad m^3/s$$

now from steam tables, $\mu = 1.8216*10^{-5}$ m^2/s

Thus

$$\mathrm{Re}_d = \frac{\rho V d}{\mu} = \frac{\rho Q d}{A_o \mu} = \frac{1.176 \times 1.139 \times 10^{-3} \times 0.008}{5.027 \times 10^{-5} \times 1.8216 \times 10^{-5}} = 11702$$

This is outside the range of the chart however it is assumed that Z_R=0.95

thus C_{DN}=0.9377 and thus **Q= 1.127 l/s**

This value is not significantly different to the last calculated value for Q thus there is no need to recalculate Re_D and this value is taken to be the solution.

The results obtained for the flow-rates using the bellmouth nozzle should not be considered highly accurate due to the deviations from the British standards, BS 1042. These results really should be considered as a rough guide only.

APPENDIX E

WIND TUNNEL CORRECTIONS

APPENDIX E

Corrections for Wind Tunnel Effects

The fact that the testing was conducted in a wind tunnel effects the results measured in the tests, the insertion of the model in the tunnel cause the flow at the working section to differ from the upstream flow. This can be attributed to the physical blockage created by the model and the development of a wake downstream of the aerofoil section. It is necessary to adjust the results obtained in order to account for these effects. The total correction factor, ε, can be expressed as the sum of the two contributing factors, that due to solid blockage, ε_{sb}, and that due to wake blockage, ε_{wb}. ie.

$$\varepsilon = \varepsilon_{wb} + \varepsilon_{sb}$$

Determination of ε_{wb}

The buoyancy correction or wake blockage correction can be determined by ignoring the solid blockage since the total correction is simply the superposition of the two terms. Assuming conditions upstream from the model section are given by velocity Vu and static pressure Pu and conditions at the working section are V and P respectively. The static pressure tappings at the front and back, top and bottom (FT, FB, BT, BB) and the contraction pressures, P1, P2, are also measured as shown in figure F.1.

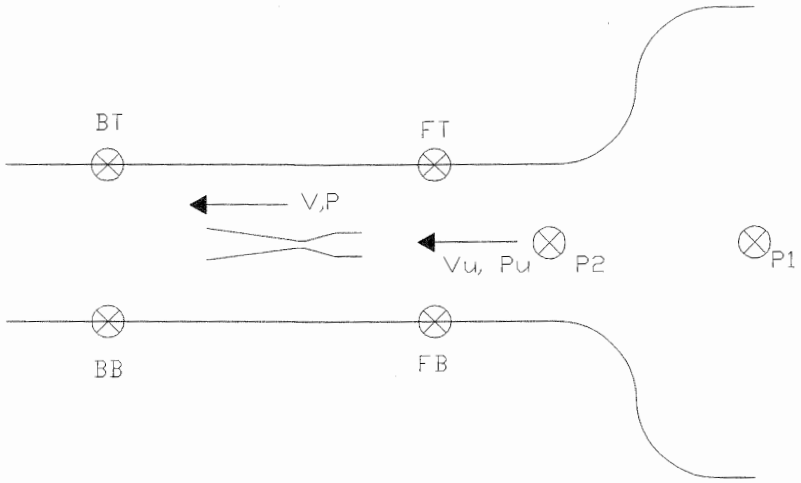

Figure F.1

Now since solid blocking is ignored the following is obtained:

$$P + \tfrac{1}{2}\rho V^2 = Pu + \tfrac{1}{2}\rho Vu^2$$

$$\therefore \frac{\tfrac{1}{2}\rho V^2}{\tfrac{1}{2}\rho Vu^2} = 1 + \frac{Pu - P}{\tfrac{1}{2}\rho Vu^2}$$

Now $V = Vu(1+\varepsilon_{wb})$ and substituting into the above equation gives:

$$\therefore \frac{Vu^2(1+\varepsilon_{wb})^2}{Vu^2} = 1 + \frac{Pu - P}{\tfrac{1}{2}\rho Vu^2}$$

if the ε_{wb}^2 term is ignored then

$$\therefore 1+\varepsilon_{wb} \cong 1+\frac{Pu-P}{\frac{1}{2}\rho V u^2}$$

which can be rearranged to give:

$$\therefore \varepsilon_{wb} \cong \frac{Pu-P}{\rho V u^2}$$

Now since $P_1 - P_2 = \frac{1}{2}\rho V u$ by calibration (to an accuracy of within 1%) the above equation simplifies to:

$$\therefore \varepsilon_{wb} \cong \frac{1}{2}\left(\frac{Pu-P}{P_1-P_2}\right)$$

It is now further assumed that:

$$Pu = \frac{1}{2}(P_{FT}+P_{FB}) \quad \text{and} \quad P = \frac{1}{4}(P_{FT}+P_{FB}+P_{BT}+P_{BB})$$

This can be described as taking average values so that the final expression for the wake blockage which includes the buoyancy correction (wall boundary layer growth) is:

$$\therefore \varepsilon_{wb} = \frac{\left(P_{FT}+P_{FB}\right)-\left(P_{BT}+P_{BB}\right)}{8\left(P_1-P_2\right)}$$

Determination of ε_{sb}

If K_3 is found for a streamline body of revolution using the figure F.2 then from the test, an appropriate expression for the solid blocking correction coefficient is:

$$\varepsilon_{sb} = \frac{\Delta V}{Vu} = \frac{K_3 \tau_1 b}{C^{3/2}}$$

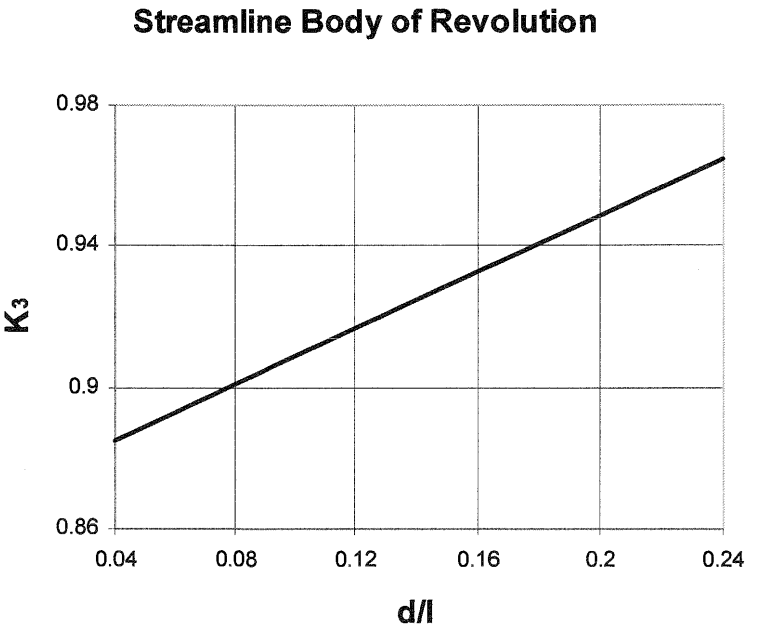

Figure F.2 - K_3 for solid body of revolution

where b = body volume

C = cross sectional area of wind tunnel

τ_1 = 0.81 for a volume of revolution in a square wind tunnel

ε_{sb} can thus be found for the tunnel. This factor is strongly dependent on the shape of the body, it is assumed that the body is a solid.:

Now C= $0.6^{2} = 0.36$

$$b = \frac{\pi d^2}{4} \times l = \frac{\pi \times 0.1^2 \times 0.667}{4} = 5.24 \times 10^{-3}$$

K_3 = .93 for cylinder attached.

$$\therefore \varepsilon_{sb} = \frac{0.93 \times 0.81 \times 5.24 \times 10^{-3}}{0.36^{3/2}} = 0.0183$$

APPENDIX F

DERIVATION OF POWER COEFFICIENT

APPENDIX F

Derivation of power coefficient

The power coefficient, C_P, of an aerogenerator is defined as the ratio of wind power available to that generated[1], this is generally written as:

$$C_P = \frac{P}{\frac{1}{2}\rho A U^3}$$

where P is the power generated by an aerogenerator and can be written as $P = \Delta p_{th} Q$ if Δp_{th} is the pressure differential between the throat and the atmosphere. Therefore

$$C_P = \frac{2\Delta p_{th} Q}{\rho A U^3} \qquad \text{.....(1)}$$

The velocity of the flow can be found in terms of the pressure tappings 1 and 2 using basic flow equations to be

---

[1] Note the difference between C_P, the power coefficient, and c_p, the coefficient of pressure.

$$p_1 - p_2 = \tfrac{1}{2}\rho U^2 \qquad \text{.....(2)}$$

(The flow through a bellmouth nozzle can be written

as $Q = C_{DN}\frac{\pi d_n^4}{4}\sqrt{\frac{2\Delta p_b}{\rho(1-m)^2}}$)..... see appendix C)

The flow through a bellmouth nozzle has been shown to be

$$Q = C_{DN} A_o \sqrt{\frac{2\Delta p_b}{\rho}} \qquad \text{.....(3)}$$

where C_{DN} is the correction factor as given by BS1042,

Δp_b is the pressure differential across the bellmouth nozzle and

A_0 is the area of the off-take tube at the pressure tapping.

By substituting (2) and (3) into (1) it is found that:

$$C_P = \frac{2\Delta p_{th}}{\rho A_i}.C_{DN} A_0 \sqrt{\frac{2\Delta p_b}{\rho}}.\left(\frac{\rho}{2(p_1 - p_2}\right)^{3/2}$$

$$= \frac{2C_{DN} A_0 \Delta p_{th}}{\rho A_i}\sqrt{\frac{\Delta p_b \rho^2}{4(p_1 - p_2)^3}}$$

$$= C_{DN} \frac{A_0}{A_i} \frac{\Delta p_{th}}{(p_1 - p_2)} \sqrt{\frac{\Delta p_b}{(p_1 - p_2)}}$$

$$= C_{DN} \frac{A_0}{A_i} \left(\frac{p_0}{(p_1 - p_2)} - \frac{p_{th}}{(p_1 - p_2)} \right) \left(\frac{p_0}{(p_1 - p_2)} - \frac{p_b}{(p_1 - p_2)} \right)^{1/2}$$

if p_0 is atmospheric pressure and p_b is the bellmouth tapping pressure.

Since c_{pi} is defined as $\frac{p_i - p_2}{p_1 - p_2}$ it can be written that

$\frac{p_0}{(p_1 - p_2)} - \frac{p_b}{(p_1 - p_2)} = \Delta c_{pb}$ where Δc_{pb} is the difference between the pressure coefficients across the bellmouth. This can also be said for the throat pressure, thus it can be shown that:

$$C_P = C_{DN} \Delta c_{pth} \frac{A_0}{A_i} \left(\Delta c_{pb} \right)^{1/2}$$

as stated.

APPENDIX G

THEORY OF FIDAP

APPENDIX G

FIDAP Analysis package

H.1 Formulation of the discrete problem

The objective of the finite element method is to reduce a continuum problem with an infinite number of degrees of freedom into a discrete problem with a finite number of degrees of freedom. For this purpose the region of interest is divided into a number of smaller regions referred to as elements. These are simply shaped in order to simplify the problem and are assumed to be fixed in space. Within each element the three variables, velocity, pressure and temperature, are assumed to be simply related to a combination of values at each node of the element. Thus it can be written that:

$$u_i(x,t) = \varphi^T \mathbf{U}_i(t)$$
$$p(x,t) = \psi^T \mathbf{P}(t)$$
$$T(x,t) = \vartheta^T \mathbf{T}(t)$$

where $\mathbf{U}_i$, $\mathbf{P}$ and $\mathbf{T}$ are column vectors of element node point unknowns and φ, ψ and ϑ are column vectors of the interpolation functions.

The equations of fluid motion written in indicial notation are:

Momentum:

$$\left(\int_V \rho_0 \varphi \varphi^T dV\right)\frac{d\mathbf{U}_i}{dt}+\left(\int_V \rho_0 \varphi u_j \frac{\partial \varphi^T}{\partial x_j} dV\right)\mathbf{U}_i-\left(\int_V \frac{\partial \varphi}{\partial x_j}\psi^T dV\right)\mathbf{P}+\left(\int_V \rho_0 \beta_T g_i \varphi \vartheta^T dV\right)\mathbf{T}$$
$$+\left(\int_V \mu \frac{\partial \varphi}{\partial x_j}\frac{\partial \varphi^T}{\partial x_j} dV\right)\mathbf{U}_i+\left(\int_V \mu \frac{\partial \varphi}{\partial x_j}\frac{\partial \varphi^T}{\partial x_i} dV\right)\mathbf{U}_j$$
$$=\int_S \sigma_i \varphi dS+\int_V \rho_0 f_i \varphi dV+\int_V \rho_0 \beta_T g_i T_0 \varphi dV$$

Continuity:
$$\left(\int_V \varphi \frac{\partial \varphi^T}{\partial x_i} dV\right)\mathbf{U}_i=0$$

Energy:
$$\left(\int_V \rho_0 c_p \vartheta \vartheta^T dV\right)\frac{d\mathbf{T}}{dt}+\left(\int_V \rho_0 c_p \vartheta u_j \frac{\partial \vartheta^T}{\partial x_j} dV\right)\mathbf{T}+\left(\int_V k \frac{\partial \vartheta}{\partial x_j}\frac{\partial \vartheta^T}{\partial x_j} dV\right)\mathbf{T}$$
$$=-\int_S (q_a+q_c+q_r)\vartheta dS+\int_V H\vartheta dV$$

Combining the momentum and energy equations into a single matrix equation we get a system of the form:

$$\begin{pmatrix}\mathbf{M}&0&0&0\\0&\mathbf{M}&0&0\\0&0&\mathbf{N}&0\\0&0&0&0\end{pmatrix}\begin{pmatrix}\dot{\mathbf{U}}_1\\\dot{\mathbf{U}}_2\\\dot{\mathbf{T}}\\\dot{\mathbf{P}}\end{pmatrix}+\begin{pmatrix}2\mathbf{K}_{11}+\mathbf{K}_{22}&\mathbf{K}_{12}&\mathbf{B}_1&-\mathbf{C}_1\\\mathbf{K}_{21}&\mathbf{K}_{11}+2\mathbf{K}_{22}&\mathbf{B}_2&-\mathbf{C}_2\\0&0&\mathbf{L}_{11}+\mathbf{L}_{22}&0\\-\mathbf{C}_1^T&-\mathbf{C}_2^T&0&0\end{pmatrix}\begin{pmatrix}\mathbf{U}_1\\\mathbf{U}_2\\\mathbf{T}\\\mathbf{P}\end{pmatrix}$$
$$+\begin{pmatrix}\mathbf{A}_1(\mathbf{U}_1)+\mathbf{A}_2(\mathbf{U}_2)&0&0&0\\0&\mathbf{A}_1(\mathbf{U}_1)+\mathbf{A}_2(\mathbf{U}_2)&0&0\\0&0&\mathbf{D}_1(\mathbf{U}_1)+\mathbf{D}_2(\mathbf{U}_2)&0\\0&0&0&0\end{pmatrix}\begin{pmatrix}\mathbf{U}_1\\\mathbf{U}_2\\\mathbf{T}\\\mathbf{P}\end{pmatrix}=\begin{pmatrix}\mathbf{F}_1\\\mathbf{F}_2\\\mathbf{G}\\0\end{pmatrix}$$

where:

$$N = \int_V \rho_0 c_p \vartheta \vartheta^T dV$$

$$A_i(U) = \int_V \rho_0 c_p \varphi u_j \frac{\partial \vartheta^T}{\partial x_i} dV$$

$$L_{ij} = \int_V k \frac{\partial \vartheta}{\partial x_i} \frac{\partial \vartheta^T}{\partial x_j} dV$$

$$\mathrm{G} = -\int_S (q_a + q_c + q_r)\vartheta dS + \int_V H \vartheta dV$$

$$M = \int_V \rho_0 \varphi \varphi^T dV$$

$$K_{ij} = \int_V \mu \frac{\partial \varphi}{\partial x_j} \frac{\partial \varphi^T}{\partial x_j} dV$$

$$C_i = \int_V \frac{\partial \varphi}{\partial x_j} \psi^T dV$$

$$D_i(U_j) = \int_V \rho_0 c_p \varphi u_j \frac{\partial \vartheta^T}{\partial x_i} dV$$

$$B_i = \int_V \rho_0 \beta_T g_i \varphi \vartheta^T dV$$

$$\mathrm{F_i} = \int_S \sigma_i \varphi dS + \int_V \rho_0 f_i \varphi dV + \int_V \rho_0 \beta_T g_i T_0 \varphi dV$$

These element matrices are spatial integrals of the various interpolation functions and their derivatives, for Newtonian fluids, 3rd order Gaussian integration can then be used to evaluate these equations.

To account for axi-symmetric flow we must add extra terms to account for the pressure matrix, **C**, and the diffusive matrix, **K**, to account for the translation between reference frames.

H.2 Boundary Conditions

Where a boundary nodal degree of freedom has been constrained then the field equation for that degree of freedom is deleted and the specified value for that node is substituted into the other equations. Where other boundary conditions are included, such as a force or flux applied to a surface, these are inserted into the momentum and energy equations at the relevant nodes.

H.3 Solution Procedure

For steady state solutions the nonlinear matrix system of equations must be solved. For this project the fixed point iteration method is used, in this case the substitution may be written as:

$$\mathbf{K}(\mathbf{u}_i)\mathbf{u}_{i+1}=\mathbf{F}$$

The nonlinearity is evaluated at $\mathbf{u}_i$ and a linear system must be formed and solved for each iteration. The advantage of the fixed point iteration method is that it is simple to understand and the radius of convergence is large meaning that it is more likely to converge than other methods, however the convergence of this method usually considerably slower that other methods available such as the Newton-Raphson method.

APPENDIX H

RAW EXPERIMENTAL DATA

Appendix H

Raw Test Data

7° Diffuser
Run 1 - Sides A and B, No Inlet Cylinder

Date:	10-Oct-96
Barometric Pressure (mPa):	1000.71
Temperature (°C):	22.50
Relative Humidity %:	45.50

Datum

P1			FB	FT	BB	BT		PA	PB	Atm	zero offset	
-12.84			-12.84	-12.92	-12.87	-12.77		-12.99	-13.01	-12.93	-12.71	
A1	A2	A3	A4	A5	A6	A8	A9	A10	A11	A12	A13	A14
-12.73	-12.78	-12.77	-12.82	-12.81	-12.69	-12.73	-12.75	-12.77	-12.78	-12.76	-12.83	-12.90
B1	B2	B3	B4	B7	B8	B9	B10	B11	B12	B13	B14	
-12.94	-12.91	-12.95	-12.89	-12.92	-12.94	-12.95	-12.82	-12.94	-13.02	-12.97	-12.97	

No Off-Take Flow

P1			FB	FT	BB	BT		PA	PB	Atm	zero offset	
193.78			-12.55	-12.51	-57.43	-53.04		174.53	174.67	174.74	-11.59	
A1	A2	A3	A4	A5	A6	A8	A9	A10	A11	A12	A13	A14
180.58	164.69	131.97	-115.09	-879.22	-879.22	-650.61	-412.18	-276.70	-207.76	-129.20	-93.67	-75.16
B1	B2	B3	B4	B7	B8	B9	B10	B11	B12	B13	B14	
179.44	164.62	133.88	-115.80	-879.22	-660.29	-413.18	-276.93	-210.32	-131.09	-94.62	-74.76	

7° Diffuser
Run 1 - Sides A and B, No Inlet Cylinder

Date:	10-Oct-96
Barometric Pressure (mPa):	1000.71
Temperature (°C):	21.80
Relative Humidity %:	45.50

Datum

P1			FB	FT	BB	BT		PA	PB	Atm	zero offset	
-13.41			-13.46	-13.36	-13.47	-13.43		-13.35	-13.54	-13.48	-13.43	
A1	A2	A3	A4	A5	A6	A8	A9	A10	A11	A12	A13	A14
-13.49	-13.57	-13.57	-13.59	-13.56	-13.42	-13.36	-13.34	-13.38	-13.33	-13.38	-13.31	-13.35
B1	B2	B3	B4	B7	B8	B9	B10	B11	B12	B13	B14	
-13.20	-13.21	-13.21	-13.21	-13.33	-13.34	-13.49	-13.35	-13.50	-13.47	-13.38	-13.37	

Full Off-Take Flow

P1			FB	FT	BB	BT		PA	PB	Atm	zero offset	
212.33			-14.98	-14.61	-64.03	-59.22		187.59	187.59	187.74	-13.51	
A1	A2	A3	A4	A5	A6	A8	A9	A10	A11	A12	A13	A14
200.84	186.50	158.56	-33.09	-686.16	-686.42	-500.26	-322.01	-219.26	-163.08	-130.37	-98.08	-79.79
B1	B2	B3	B4	B7	B8	B9	B10	B11	B12	B13	B14	
199.29	186.23	160.12	-34.27	-686.42	-510.78	-322.50	-223.69	-169.15	-132.77	-98.96	-79.83	

7° Diffuser
Run 2 - Sides C and D, No Inlet Cylinder

Date:	10-Oct-96
Barometric Pressure (mPa):	1000.18
Temperature (°C):	22.40
Relative Humidity %:	48.70

Datum

P1			FB	FT	BB	BT			PA	Atm	zero offset		
-14.34			-14.28	-14.30	-14.30	-14.23			-14.27	-14.20	-14.30		
C1	C2	C3	C4	C5	C6	C7	C8	C9	C10	C11	C12	C13	C14
-14.22	-14.26	-14.20	-14.26	-14.19	-14.21	-14.20	-14.19	-14.20	-14.19	-14.22	-14.21	-14.31	-14.26
D1	D2	D3	D4	D5	D6	D7	D8	D9	D10	D11	D12	D13	D14
-14.26	-14.27	-14.27	-14.26	-14.22	-14.23	-14.29	-14.31	-14.27	-14.29	-14.34	-14.31	-14.23	-14.26

No Off-Take Flow

P1			FB	FT	BB	BT			PA	Atm	zero offset		
195.53			-15.74	-15.33	-64.34	-58.69			-156.97	177.31	-14.54		
C1	C2	C3	C4	C5	C6	C7	C8	C9	C10	C11	C12	C13	C14
180.78	166.10	131.93	-131.73	-878.23	-878.37	-878.38	-697.06	-438.75	-292.12	-221.96	-139.01	-100.67	-80.01
D1	D2	D3	D4	D5	D6	D7	D8	D9	D10	D11	D12	D13	D14
180.02	164.04	130.93	-141.84	-878.38	-878.38	-878.38	-689.95	-437.96	-295.83	-221.22	-137.70	-100.81	-80.77

Full Off-Take Flow

P1			FB	FT	BB	BT			PA	Atm	zero offset		
196.89			-15.73	-15.11	-65.01	-59.38			-160.68	175.65	-14.38		
C1	C2	C3	C4	C5	C6	C7	C8	C9	C10	C11	C12	C13	C14
184.51	172.87	146.18	-44.15	-686.40	-686.42	-686.42	-485.97	-315.96	-216.72	-164.02	-129.63	-96.35	-78.12
D1	D2	D3	D4	D5	D6	D7	D8	D9	D10	D11	D12	D13	D14
183.88	170.98	144.74	-49.85	-686.42	-686.42	-686.42	-483.13	-318.44	-217.97	-164.29	-129.18	-95.28	-78.28

7° Diffuser
Run 3, Inlet Cylinder

Date: 18-Oct-96
Barometric Pressure (mPa): 1002.50
Temperature (°C): 21.00
Relative Humidity %: 38.35

Datum

P1			FB	FT	BB	BT			PA	atm	zero offset		
-13.12			-13.23	-13.15	-13.13	-13.15			-13.09	-13.08	-13.15		
C1	C2	C3	C4	C5	C6	C7	C8	C9	C10	C11	C12	C13	C14
-13.08	-13.10	-13.08	-13.07	-13.06	-13.06	-13.03	-13.07	-12.12	-13.02	-13.01	-13.06	-13.05	-13.06
D1	D2	D3	D4	D5	D6	D7	D8	D9	D10	D11	D12	D13	D14
-13.08	-13.12	-13.13	-13.09	-13.10	-13.08	-13.07	-13.09	-13.08	-13.06	-13.07	-13.09	-13.06	-13.1

No Off-Take Flow

P1			FB	FT	BB	BT			PA	atm	zero offset		
208.92			-14.84	-14.01	-61.08	-55.34			-207.61	144.40	-12.73		
C1	C2	C3	C4	C5	C6	C7	C8	C9	C10	C11	C12	C13	C14
190.77	175.48	139.55	-111.29	-878.90	-878.90	-878.90	-604.58	-452.47	-301.75	-231.57	-179.75	-128.85	-98.35
D1	D2	D3	D4	D5	D6	D7	D8	D9	D10	D11	D12	D13	D14
190.77	176.36	142.20	-112.21	-878.90	-878.90	-595.73	-378.18	-171.39	-108.31	57.84	40.11	94.02	-72.04

Full Off-Take Flow

P1			FB	FT	BB	BT			PA	atm	zero offset		
208.37			-15.77	-14.98	-62.46	-56.73			-211.61	146.27	-13.53		
C1	C2	C3	C4	C5	C6	C7	C8	C9	C10	C11	C12	C13	C14
194.41	181.74	153.56	-45.65	-686.42	-686.42	-686.42	-503.11	-322.39	-222.85	-167.02	-132.66	-96.95	-78.76
D1	D2	D3	D4	D5	D6	D7	D8	D9	D10	D11	D12	D13	D14
194.41	183.50	156.03	-44.40	-686.42	-686.42	-686.56	-271.88	-123.75	-77.73	44.56	29.64	72.18	-65.02

13° Diffuser
Run 1 - Sides A and B, No Inlet Cylinder

Date:	11-Oct-96
Barometric Pressure (mPa):	997.78
Temperature (°C):	20.50
Relative Humidity %:	51.80

Datum

P1			FB	FT	BB	BT		PA	PB	Atm	zero offset	
-4.58			-4.59	-4.60	-4.65	-4.60		-4.82	-4.80	-4.57	-4.56	
A1	A2	A3	A4	A5	A6	A8	A9	A10	A11	A12	A13	A14
-4.68	-4.66	-4.68	-4.68	-4.67	-4.66	-4.67	-4.66	-4.67	-4.65	-6.82	-4.68	-4.66
B1	B2	B3	B4	B7	B8	B9	B10	B11	B12	B13	B14	
-4.65	-4.66	-4.67	-4.67	-4.66	-4.61	-4.64	-4.63	-4.65	-4.65	-4.64	-4.61	

No Off-Take Flow

P1			FB	FT	BB	BT		PA	PB	Atm	zero offset	
218.58			-5.88	-5.20	-66.30	-59.78		199.88	199.87	199.80	-4.32	
A1	A2	A3	A4	A5	A6	A8	A9	A10	A11	A12	A13	A14
208.03	199.15	177.08	26.53	-509.07	-520.21	-219.83	-176.37	-149.96	-138.18	-116.33	-106.59	-102.10
B1	B2	B3	B4	B7	B8	B9	B10	B11	B12	B13	B14	
209.02	198.82	177.93	22.08	-342.20	-216.55	-206.05	-154.24	-138.18	-120.74	-103.96	-98.56	

Full Off-Take Flow

P1			FB	FT	BB	BT		PA	PB	Atm	zero offset	
219.01			-6.29	-5.60	-65.87	-59.57		197.82	198.14	198.32	-4.72	
A1	A2	A3	A4	A5	A6	A8	A9	A10	A11	A12	A13	A14
210.31	202.78	185.91	70.21	-350.15	-389.10	-179.66	-147.56	-133.91	-125.59	-113.78	-110.15	-108.28
B1	B2	B3	B4	B7	B8	B9	B10	B11	B12	B13	B14	
210.66	202.51	186.68	68.30	-321.91	-196.64	-165.28	-136.56	-125.59	-116.00	-109.11	-105.17	

13° Diffuser
Run 2 - Sides C and D, No Inlet Cylinder

Date:	11-Oct-96
Barometric Pressure (mPa):	998.32
Temperature (°C):	19.18
Relative Humidity %:	52.88

Datum

P1			FB	FT	BB	BT			PA	Atm	zero offset		
-2.34			-2.31	-2.24	-2.27	-2.23			-2.43	-2.33	-2.22		
C1	C2	C3	C4	C5	C6	C7	C8	C9	C10	C11	C12	C13	C14
-2.32	-2.31	-2.30	-2.32	-2.33	-2.38	-2.38	-2.39	-2.36	-2.38	-2.39	-2.44	-2.41	-2.422
D1	D2	D3	D4	D5	D6	D7	D8	D9	D10	D11	D12	D13	D14
-2.22	-2.23	-2.30	-2.28	-2.36	-2.32	-2.30	-2.30	-2.31	-2.35	-2.31	-2.28	-2.32	-2.418

No Off-Take Flow

P1			FB	FT	BB	BT			PA	Atm	zero offset		
214.23			-2.79	-2.21	-59.83	-54.36			87.13	195.60	-1.27		
C1	C2	C3	C4	C5	C6	C7	C8	C9	C10	C11	C12	C13	C14
204.35	194.72	172.09	17.50	-525.96	-507.68	-400.38	-209.19	-182.97	-147.85	-128.72	-114.39	-94.19	-89.47
D1	D2	D3	D4	D5	D6	D7	D8	D9	D10	D11	D12	D13	D14
203.44	193.73	171.89	18.79	-496.13	-489.01	-380.75	-215.43	-181.87	-152.26	-128.44	-112.70	-95.48	-88.17

Full Off take Flow

P1			FB	FT	BB	BT			PA	Atm	zero offset		
216.05			-3.46	-2.89	-59.97	-54.58			83.79	194.43	-2.00		
C1	C2	C3	C4	C5	C6	C7	C8	C9	C10	C11	C12	C13	C14
208.59	201.10	185.00	73.82	-330.00	-363.16	-337.48	-179.52	-150.86	-123.75	-117.11	-106.20	-99.53	-99.66
D1	D2	D3	D4	D5	D6	D7	D8	D9	D10	D11	D12	D13	D14
207.91	200.62	183.98	69.69	-326.15	-378.75	-350.61	-180.29	-146.09	-129.55	-114.70	-106.91	-100.71	-96.95

13° Diffuser
Run 3, Inlet Cylinder

Date:	18-Oct-96
Barometric Pressure (mPa):	1002.00
Temperature (°C):	21.85
Relative Humidity %:	37.90

Datum

P1			FB	FT	BB	BT			PA	atm	zero offset		
-14.90			-14.87	-14.98	-14.92	-14.96			-14.92	-14.97	-14.93		
C1	C2	C3	C4	C5	C6	C7	C8	C9	C10	C11	C12	C13	C14
-14.86	-14.97	-15.02	-14.99	-14.95	-14.97	-14.97	-14.96	-14.97	-14.96	-14.98	-14.94	-14.98	-14.95
D1	D2	D3	D4	D5	D6	D7	D8	D9	D10	D11	D12	D13	D14
-14.93	-14.86	-14.95	-14.92	-14.93	-14.91	-14.95	-14.94	-14.95	-14.96	-14.82	-14.86	-14.91	-14.94

No Off-Take Flow

P1			FB	FT	BB	BT			PA	atm	zero offset		
208.76			-17.42	-16.67	-74.68	-68.42			36.60	163.52	-15.30		
C1	C2	C3	C4	C5	C6	C7	C8	C9	C10	C11	C12	C13	C14
188.32	186.86	165.12	-1.70	-532.70	-560.98	-442.01	-333.30	-208.96	-165.50	-143.67	-128.61	-108.74	-103.4
D1	D2	D3	D4	D5	D6	D7	D8	D9	D10	D11	D12	D13	D14
196.87	188.32	166.86	4.90	-553.18	-528.35	-391.30	-166.61	-83.22	-66.17	-61.33	23.12	78.71	62.324

Full Off-Take Flow

P1			FB	FT	BB	BT			PA	atm	zero offset		
211.84			-17.92	-17.11	-74.61	-68.44			39.54	164.45	-15.63		
C1	C2	C3	C4	C5	C6	C7	C8	C9	C10	C11	C12	C13	C14
195.02	194.92	179.09	66.18	-364.02	-400.31	-372.85	47.55	-164.62	-142.34	-129.22	-121.72	-114.28	-113.9
D1	D2	D3	D4	D5	D6	D7	D8	D9	D10	D11	D12	D13	D14
201.40	195.02	178.74	63.06	-338.02	-372.56	98.03	-133.16	-61.09	-56.69	-43.29	19.20	77.79	65.365

10° Diffuser
Run 1, No Inlet Cylinder

Date:	18-Oct-96
Barometric Pressure (mPa):	998.40
Temperature (°C):	23.13
Relative Humidity %:	31.70

Datum

P1			FB	FT	BB	BT			PA	atm	zero offset	
-23.50			-23.50	-23.48	-23.44	-23.46			-23.47	-23.52	-23.50	
C1	C2	C3	C4	C5	C6	C7	C9	C10	C11	C12	C13	C14
-23.47	-23.46	-23.46	-23.50	-23.46	-23.47	-23.44	-23.47	-23.45	-23.47	-23.47	-23.44	-23.45
D1	D2	D3	D4	D5	D6	D7	D9	D10	D11	D12	D13	D14
-23.45	-23.47	-23.45	-23.47	-23.43	-23.43	-23.44	-23.44	-23.46	-23.49	-23.48	-23.44	-23.46

No Off-Take Flow

P1			FB	FT	BB	BT			PA	atm	zero offset	
198.37			-24.53	-22.86	-70.86	-65.61			-59.90	183.85	-22.41	
C1	C2	C3	C4	C5	C6	C7	C9	C10	C11	C12	C13	C14
156.54	164.99	129.41	-121.71	-686.42	-686.42	-686.42	-278.81	-196.90	-175.63	-99.00	-106.28	-27.43
D1	D2	D3	D4	D5	D6	D7	D9	D10	D11	D12	D13	D14
171.58	156.54	128.22	-77.51	-686.42	-686.42	-686.42	-285.73	-213.66	-175.43	-145.39	-116.29	-100.18

Full off-Take Flow

P1			FB	FT	BB	BT			PA	atm	zero offset	
198.07			-24.55	-23.01	-71.52	-66.10			-59.98	181.62	-22.38	
C1	C2	C3	C4	C5	C6	C7	C9	C10	C11	C12	C13	C14
165.69	175.32	153.19	-3.54	-626.44	-672.51	-608.48	-233.07	-164.39	-150.34	-83.37	-98.52	-23.53
D1	D2	D3	D4	D5	D6	D7	D9	D10	D11	D12	D13	D14
177.54	165.69	150.04	9.04	-605.29	-628.35	-597.47	-240.19	-196.08	-161.25	-135.43	-106.07	-94.89

5° Diffuser
Run 1, No Inlet Cylinder

Date:	16-Oct-96
Barometric Pressure (mPa):	751.90
Temperature (°C):	25.20
Relative Humidity %:	28.00

Datum

P1			FB	FT	BB	BT			PA	atm	zero offset	
-23.17			-23.22	-23.12	-23.19	-23.17			-23.13	-23.21	-23.22	
C1	C2	C3	C4	C5	C6	C7	C9	C10	C11	C12	C13	C14
-23.26	-23.25	-23.22	-23.18	-23.19	-23.21	-23.23	-23.23	-23.20	-23.20	-23.18	-23.19	-23.24
D1	D2	D3	D4	D5	D6	D7	D9	D10	D11	D12	D13	D14
-23.21	-23.20	-23.23	-23.27	-23.25	-23.22	-23.12	-23.22	-23.17	-23.09	-23.01	-23.03	-23.13

No Off-Take Flow

P1			FB	FT	BB	BT			PA	atm	zero offset	
231.43			15.44	-17.99	-27.42	-24.73			-2.48	193.20	16.87	
C1	C2	C3	C4	C5	C6	C7	C9	C10	C11	C12	C13	C14
213.12	203.34	178.86	6.12	-291.70	-627.77	-696.54	-287.27	-195.50	-150.32	-90.31	-73.22	-47.18
D1	D2	D3	D4	D5	D6	D7	D9	D10	D11	D12	D13	D14
212.89	204.30	179.40	9.63	-706.41	-706.41	-706.41	-289.87	-197.58	-150.31	-90.17	-73.03	-47.39

Full Off-Take Flow

P1			FB	FT	BB	BT			PA	atm	zero offset	
231.58			15.35	-17.88	-27.10	-24.09			-2.49	190.22	16.79	
C1	C2	C3	C4	C5	C6	C7	C9	C10	C11	C12	C13	C14
213.25	203.88	185.69	63.03	-245.67	-454.05	-570.27	-238.43	-164.06	-133.92	-112.94	-91.99	-80.96
D1	D2	D3	D4	D5	D6	D7	D9	D10	D11	D12	D13	D14
212.73	203.03	184.03	97.02	-606.42	-606.42	-606.42	-240.90	-166.46	-134.39	-112.79	-91.96	-81.28

APPENDIX I

CALLIBRATION OF WIND TUNNEL VELOCITY

Appendix I

Tunnel Velocity Callibration

Date	18-Oct-96
Temperature, °C:	24.2
Barometric Pressure, mPa:	998.4
Relative Humidity:	30.1%

thus from psychrometric chart:

ρ =	1.1765 kg/m3

Raw Data

distance from wall	Pressures			
	P1-P2	Static	Dynamic	Zero Offset
d/2	269.3324	-7.790	267.425	-11.510
.3d/2	269.0432	-7.934	270.834	-11.550
.6d/2	269.3438	-7.979	268.392	-11.581
datum	-11.43465	-11.456	-11.453	

Corrected Data

distance from wall	P1-P2	Velocity		Static	Dynamic	Velocity		Error
d/2	280.842	21.850		3.720	278.935	21.630		1.02%
.3d/2	280.593	21.841		3.616	282.383	21.769		0.33%
.6d/2	280.924	21.853		3.601	279.973	21.676		0.82%

APPENDIX J

CALCULATION OF OFF-TAKE FLOW RATE

Appendix J

Offtake Flow Rate Calculation:

Dimensions:
d= 0.008
A_0= 5.027E-05

	7 ° - no cylinder	7° with cylinder	13° - no cylinder	13° with cylinder	10° no cylinder	5° no cylinder
Test Data:						
Temperature:	21.95	21.00	20.50	22.30	24.00	25.20
Relative Humidity:	45.52	36.60	51.40	37.90	31.40	28.00
Pressure:	1000.71	1002.50	997.78	1002.00	998.40	1002.45
P_A	-146.33	-198.14	85.99	55.17	-37.63	-19.36
P_{atm}	189.93	159.74	196.54	180.13	204.02	173.42
Δp	336.26	357.88	110.55	124.96	241.65	192.79
density(kg/m^3)	1.19	1.20	1.20	1.19	1.18	1.17
viscosity	1.82E-05	1.82E-05	1.82E-05	1.82E-05	1.83E-05	1.80E-05

C=	0.987
Z_D=	1
ε=	1

Assume Z_{Re}=	0.96	0.96	0.96	0.96	0.96	0.96
C_{DN}	0.948	0.948	0.948	0.948	0.948	0.948
Q=	1.13E-03	1.16E-03	6.47E-04	6.91E-04	9.64E-04	8.65E-04
Re_d	11771.83	12207.46	6795.85	7155.79	9876.74	8932.93
Now Z_{Re} =	0.95	0.95	0.95	0.95	0.95	0.95
CDN	0.938	0.938	0.938	0.938	0.938	0.938
Volumetric Flowrate:	**1.12E-03**	**1.15E-03**	**6.40E-04**	**6.84E-04**	**9.54E-04**	**8.56E-04**

APPENDIX K

LOSSES ASSOCIATED WITH THE SYSTEM

Appendix K

Losses Associated With The System

	Section	Diameter (m)	k	k*	k^*/d^4
INLET:	inlet	0.055	0.5	0.5	53853
	pipe 1	0.055	0.0818	0.0818	8810
	bend	0.055	0.95	0.95	102322
	pipe 2	0.055	0.0458	0.0458	4933
	pipe 3	0.055	0.406	0.406	43729
T-JUNCTION	T junction	0.055	2.2	2.2	236955
	pipe 4	0.055	0.259	0.06475	6974
	outlet	0.055	1	0.25	26927
CHAMBER					25356
OUTLET	inlet	0.100	0.53	0.53	5300
	pipe 1	0.100	0.067	0.067	670
	bend	0.100	0.57	0.57	5700
	pipe 2	0.100	0.45	0.45	4500
	contraction	0.055	0.44	0.44	47391
	pipe 3	0.055	0.067	0.067	7216
	outlet	0.055	0.53	0.53	57085
	offtake	0.055	0.2	0.2	21541
				Σ	**659263**

Without T-junction:

	Section	Diameter (m)	k	k*	k^*/d^4
INLET:	inlet	0.055	0.5	0.5	53853
	pipe 1	0.055	0.0818	0.0818	8810
	bend	0.055	0.95	0.95	102322
	pipe 2	0.055	0.0458	0.0458	4933
	pipe 3	0.055	0.406	0.406	43729
T-JUNCTION	T junction	0.055	0	0	0
	pipe 4	0.055	0.259	0.259	27896
	outlet	0.055	1	1	107707
CHAMBER					25356
OUTLET	inlet	0.100	0.53	0.53	5300
	pipe 1	0.100	0.067	0.067	670
	bend	0.100	0.57	0.57	5700
	pipe 2	0.100	0.45	0.45	4500
	contraction	0.055	0.44	0.44	47391
	pipe 3	0.055	0.067	0.067	7216
	outlet	0.055	0.53	0.53	57085
	offtake	0.055	0.2	0.2	21541
				Σ	**524010**

APPENDIX L

CORRECTED PRESSURE COEFFICIENTS

Appendix L

Corrected Pressure Coefficients

15° Diffuser With Inlet Cylinder

No Off-Take Flow:

ε_{sb}=	0.0183
ε_{wb}=	0.0608
$1+\varepsilon_{sb}+\varepsilon_{wb}$=	1.0791

Position	0.202	0.243	0.280	0.336	0.391	0.408	0.450
Pressure Coefficient	1.001	0.977	0.873	0.082	-2.541	-2.550	-1.933

Position	0.502	0.565	0.637	0.712	0.787	0.900	0.990
Pressure Coefficient	-1.130	-0.630	-0.484	-0.420	-0.180	0.001	-0.025

Full Off-Take Flow

ε_{sb}=	0.0183
ε_{wb}=	0.0594
$1+\varepsilon_{sb}+\varepsilon_{wb}$=	1.0777

Position	0.202	0.243	0.280	0.336	0.391	0.408	0.450
Pressure Coefficient	1.013	0.998	0.922	0.380	-1.589	-1.757	-1.239

Position	0.502	0.565	0.637	0.712	0.787	0.900	0.990
Pressure Coefficient	-0.560	-0.460	-0.397	-0.335	-0.169	-0.012	-0.041

7° Diffuser With Inlet Cylinder

No Off-Take Flow:

ε_{sb}=	0.0183
ε_{wb}=	0.0494
$1+\varepsilon_{sb}+\varepsilon_{wb}$=	1.0677

Position	0.202	0.243	0.280	0.336	0.391	0.408	0.450
Pressure Coefficient	0.980	0.909	0.740	-0.477	-4.173	-4.173	-4.173

Position	0.502	0.565	0.637	0.712	0.787	0.900	0.990
Pressure Coefficient	-3.491	-2.306	-1.444	-0.927	-0.358	-0.275	-0.023

Full Off-Take Flow

ε_{sb}=	0.0183
ε_{wb}=	0.0499
$1+\varepsilon_{sb}+\varepsilon_{wb}$=	1.0682

Position	0.202	0.243	0.280	0.336	0.391	0.408	0.450
Pressure Coefficient	1.001	0.944	0.810	-0.152	-3.240	-3.240	-3.240

Position	0.502	0.565	0.637	0.712	0.787	0.900	0.990
Pressure Coefficient	-1.801	-1.011	-0.659	-0.230	-0.183	0.005	-0.281

APPENDIX M

DETERMINATION OF POWER COEFFICIENT

Appendix M

Determination of Power Coefficient

$D_{bellmouth}$= 0.008

D_{inlet}= 0.100

C_{DN} = 0.938

Pressure Coefficients:	p_{Atm}	p_{throat}	$P_{bellmouth}$	C_P
7° no cylinder	0.899	-3.181	-0.693	**0.031**
7° cylinder	0.720	-3.033	-0.893	**0.029**
15° no cylinder	0.901	-1.503	0.394	**0.010**
15° cylinder	0.792	-1.532	0.243	**0.010**
5° no cylinder	0.808	-1.222	-0.090	**0.012**
10° no cylnder	0.925	-2.740	-0.171	**0.023**